Iridium-Catalyzed Hydrogenation of N-Heterocyclic Compounds under Mild Conditions by an Outer-Sphere Pathway

Graham E. Dobereiner,[†] Ainara Nova,[‡,§] Nathan D. Schley,[†] Nilay Hazari,[†] Scott J. Miller,[†] Odile Eisenstein,*,[‡] and Robert H. Crabtree*,[†]

[†]Department of Chemistry, Yale University, 225 Prospect Street, P.O. Box 208107, New Haven, Connecticut 06520, United States
[‡]Institut Charles Gerhardt, Université Montpellier 2, CNRS UMR 5253, cc 1501, Place E. Bataillon, 34095, Montpellier, France

S *Supporting Information*

ABSTRACT: A new homogeneous iridium catalyst gives hydrogenation of quinolines under unprecedentedly mild conditions—as low as 1 atm of H_2 and 25 °C. We report air- and moisture-stable iridium(I) NHC catalyst precursors that are active for reduction of a wide variety of quinolines having functionalities at the 2-, 6-, and 8- positions. A combined experimental and theoretical study has elucidated the mechanism of this reaction. DFT studies on a model Ir complex show that a conventional inner-sphere mechanism is disfavored relative to an unusual stepwise outer-sphere mechanism involving sequential proton and hydride transfer. All intermediates in this proposed mechanism have been isolated or spectroscopically characterized, including two new iridium(III) hydrides and a notable cationic iridium(III) dihydrogen dihydride complex. DFT calculations on full systems establish the coordination geometry of these iridium hydrides, while stoichiometric and catalytic experiments with the isolated complexes provide evidence for the mechanistic proposal. The proposed mechanism explains why the catalytic reaction is slower for unhindered substrates and why small changes in the ligand set drastically alter catalyst activity.
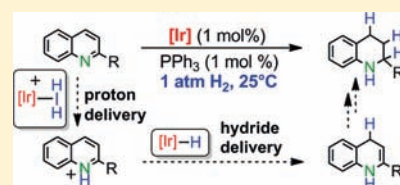
■ INTRODUCTION

The hydrogenation of nitrogen heterocycles, including quinolines, is of current interest.[1,2] The tetrahydroquinoline core, formed from quinoline hydrogenation, is present in many natural products and pharmaceuticals, and direct hydrogenation is an efficient route to tetrahydroquinolines and other saturated N-heterocycles.[1] Furthermore, we and others have recently proposed nitrogen-containing heterocyclic liquids as hydrogen storage materials that may be safer than metal hydrides, but more efficient hydrogenation catalysts are needed to achieve this goal.[2]

Many homogeneous catalysts can reduce isolated C=C, C=O, and C=N double bonds in olefins, carbonyls, and imines, but hydrogenation of nitrogen-containing aromatics is more challenging. Homogeneous N-heterocycle hydrogenation has proved possible with many Rh, Ru, Ir, and Os catalyst precursors,[3-6] including asymmetric hydrogenation catalysts for quinoline conversion to tetrahydroquinolines.[7-14] Unfortunately, almost all quinoline hydrogenation catalysts require either high pressures or elevated temperatures. For example, homogeneous iridium catalysts for the room-temperature hydrogenation of quinolines typically require an excess of 15 atm of H_2 for good conversions, while catalysts that operate at lower hydrogen pressures require elevated temperatures (~100 °C or higher).[5,6] In addition, many systems require the presence of harsh additives such as I_2.

Rational design of quinoline hydrogenation catalysts is difficult, because there have only been a few mechanistic studies and in some cases closely related systems have even given contradictory results.[15] Despite the array of inner-sphere and outer-sphere mechanisms that have been proposed for the hydrogenation reactions or hydrogen transfer reactions of polar bonds,[16] almost all current proposals for quinoline hydrogenation reactions (Scheme 1) assume inner-sphere coordination of substrate. For example, Fish suggested that a $[(Cp^*)Rh(MeCN)_3]^{2+}$ precatalyst formed an imperfectly defined Cp*Rh hydride intermediate which could insert into the bound quinoline C=N double bond and then reductively eliminate the hydrogenated product.[4] A similar pathway has been proposed for a number of catalysts, such as $[Rh(cod)(PPh_3)_2]PF_6$ by Sanchez-Delgado et al.,[5] an iridium triphos system by Rosales et al.,[17] and a rhodium tripodal polyphosphine complex by Bianchini et al.[18] Rosales' CNDO2 calculations suggest that C=N bond reduction in a model of $[RuH(CO)(MeCN)_2(PR_3)_2]^+$ occurs through a redox-neutral cycle,[19] with 1,2-hydride insertion into the bound substrate, followed by heterolytic H_2 cleavage to liberate substrate and regenerate the hydride. Zhou et al. also suggested a redox-neutral cycle involving heterolytic H_2 cleavage, but they proposed a 1,4- rather than 1,2-hydride insertion.[13] In contrast to these mechanisms, Chan recently proposed an outer-sphere mechanism, which involved proton transfer from a Ru dihydrogen complex to the substrate followed by hydride transfer to the protonated substrate.[8] This type of sequential mechanism is unusual and is rarely invoked for the hydrogenation of organic substrates.[20]

Scheme 1. Prior Mechanistic Proposals for the Hydrogenation of Quinolines[4,8,19]

Fish, 1992:

Rosales, 1998:

Chan, 2008:
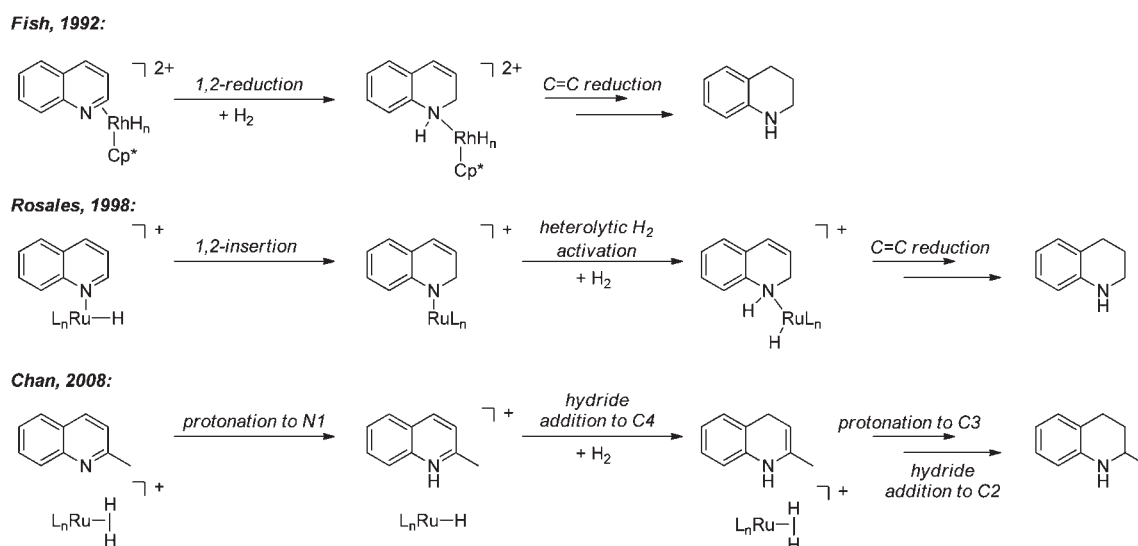
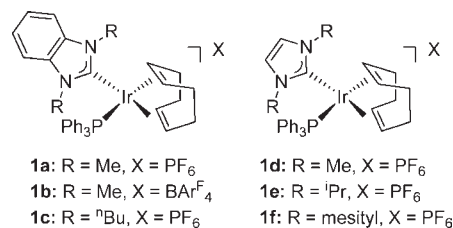**Scheme 2. Synthesis of the Precursor 1a**
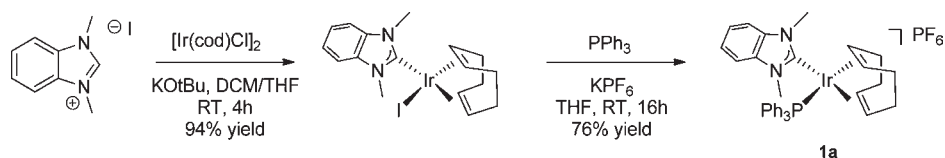
We now describe a new air- and moisture-stable, homogeneous catalyst for the hydrogenation of aza-heterocycles having unprecedented activity at ambient temperature and hydrogen pressures as low as 1 atm of H_2. Our mild conditions have facilitated a detailed mechanistic study. Both experimental and computational results suggest that the hydrogenation does not involve direct coordination of the substrate to Ir; instead, we propose that the reaction proceeds via an unusual stepwise outer-sphere pathway that includes a key dihydrogen complex. Each of the intermediates in our stepwise mechanism has been isolated or spectroscopically characterized.

Chart 1. Iridium Precursor Complexes Screened for Catalytic Activity

1a: R = Me, X = PF_6
1b: R = Me, X = BAr^F_4
1c: R = ^nBu, X = PF_6

1d: R = Me, X = PF_6
1e: R = ^iPr, X = PF_6
1f: R = mesityl, X = PF_6

RESULTS AND DISCUSSION

Synthesis of Iridium(I) Precursor Complexes. No reports of N-heterocyclic carbenes (NHCs) as ancillary ligands in quinoline hydrogenation catalysts have appeared,[21] although NHCs do feature in several olefin hydrogenation catalysts.[22,23] Iridium-based catalysts are some of the most active for hydrogenation, especially those based on the (cod)Ir[I] fragment (cod = 1,5-cyclooctadiene).[24] We therefore began by synthesizing a series of Ir(I) NHC phosphine complexes, a class first reported by Buriak.[23]

We first prepared neutral iridium NHC species either through base-assisted NHC metalation[25] from an imidazolium salt and [Ir(cod)Cl]$_2$ or by transmetalation from a silver carbene.[26] The resulting neutral [Ir(cod)(NHC)X] compounds react with neutral ligands in the presence of the noncoordinating anion X to yield ionic [Ir(cod)(NHC)L]X species such as **1a** (a representative synthesis is shown in Scheme 2). As found by Buriak,[23] these convenient precursors are air stable both in the solid state and in solution and thus require no special handling, and the purification of the cationic complexes can be performed in air without any loss in yield.

Six different ionic complexes were synthesized (Chart 1), of which only **1d,f** were previously known.[23,27] Benzimidazole- and imidazole-based NHCs with various wingtip substitutions were included. The analogue of **1a** with the noncoordinating anion BAr^F_4 (**1b**; BAr^F_4 = tetrakis[3,5-bis(trifluoromethyl)-phenyl]borate) was also prepared, as this anion has been reported to improve the efficiency of olefin hydrogenation catalysts versus PF_6.[28] All the new Ir complexes were fully characterized, and the structure of **1a** was confirmed by X-ray crystallography (Figure 1). As expected, the geometry around Ir in **1a** is square planar and bond lengths and angles are consistent with those reported for **1f**.[27]

Catalyst Optimization. Initial screens at high hydrogen pressures (70 atm) in toluene at room temperature (Table 1) used 2-methylquinoline as the substrate with catalyst **1a**. Complex **1a** is indeed capable of generating trace amounts of 2-methyl-1,2,3,4-tetrahydroquinoline, but without appreciable catalytic turnover. In contrast to the case for some earlier catalysts,[12,14] stoichiometric iodide does not increase yields. Superstoichiometric quantities of KPF_6 and HBF_4 also had no effect. However, the addition of triphenylphosphine greatly improved activity. In this case, we observed good conversions
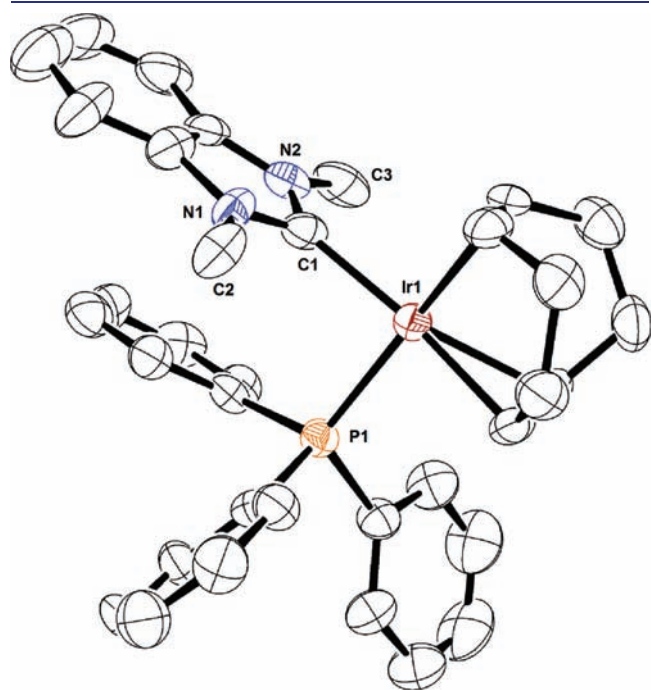
Figure 1. Crystal structure of catalyst precursor **1a** (hydrogen atoms and anion omitted for clarity). Selected bond lengths (Å) and angles (deg): Ir(1)−P(1) = 2.3215(17), Ir(1)−C(1) = 2.042(7), N(1)−C(1) = 1.365(8), N(1)−C(2) = 1.458(10), N(2)−C(1) = 1.347(9), N(2)−C(3) = 1.447(9); P(1)−Ir(1)−C(1) = 89.5(2), C(1)−N(1)−C(2) = 126.0(7), C(1)−N(2)−C(3) = 124.4(7), Ir(1)−C(1)−N(1) = 127.1(5), Ir(1)−C(1)−N(2) = 127.15.

even at 1 atm of H_2 at reasonable reaction times (<24 h). The activity was solvent dependent, with high conversions observed in toluene, in which the precatalyst is sparingly soluble, and trifluorotoluene, in which the precatalyst is fully soluble. Reactions in other solvents or solvent mixtures failed to generate any product.

A screen of **1a**−**f** (Chart 1) indicated that the ancillary NHC ligand is crucial (Table 2). We performed hydrogenation reactions in both toluene and trifluorotoluene for each iridium precursor. In general, trifluorotoluene gave higher conversions than toluene, presumably due to the greater solubility of the iridium complexes in this solvent. In toluene poorer product conversions were obtained when the PF_6 salt (**1a**) was replaced with the BAr^F_4 salt (**1b**); however, both were very active in trifluorotoluene. Complex **1c**, which features a benzimidazole NHC with butyl wingtips, gave low conversion in both solvents. The imidazole-based NHC complex **1d** was inactive in toluene and somewhat active in trifluorotoluene, while the related imidazole-based complexes **1e,f** gave no conversion to the 2-methyltetrahydroquinoline product in either solvent. This may be due to the greater steric demand of the isopropyl and mesityl wingtips. The versatility of **1a** allowed us to perform our substrate screen in toluene, which has a lower cost and greater availability than trifluorotoluene.

Overall, our screening reactions with NHC Ir(I) precatalysts resulted in a system that can hydrogenate 2-methylquinoline

Table 2. Screening of Iridium Precursors for Quinoline Hydrogenation under Optimized Conditions[a]

complex	time, h	conversion,[b] %
1a	18	>95 (>95)[c]
1b	18	59 (>95)
1c	18	15 (30)
1d	18	0 (18)
1e	18	0 (0)
1f	18	0 (0)

[a] Conditions: 2-methylquinoline (1 equiv), Ir complex (1 mol %), PPh_3 (1 mol %), 1 atm of H_2, 35 °C, 18 h. [b] The percent product conversion was obtained by NMR integration of the product and any starting material remaining and normalizing to 100%. [c] Values in parentheses are conversions in trifluorotoluene.

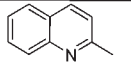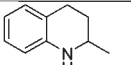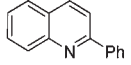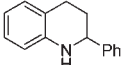**Table 1. Initial Optimization of the Hydrogenation of 2-Methylquinoline**
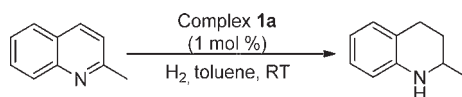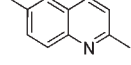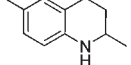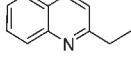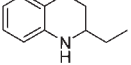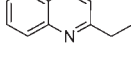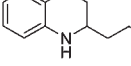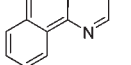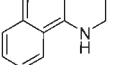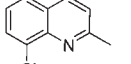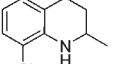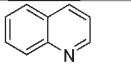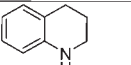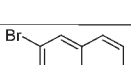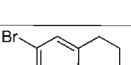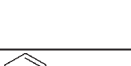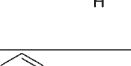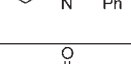
additive (amt)	solvent	pressure of H_2, atm	time, h	conversion,[a] %
KI (5 equiv)	toluene	70	24	<5
50% HBF_4 (5 equiv)[b]	toluene	70	24	<5
KPF_6 (5 equiv)	toluene	70	24	<5
PPh_3 (1 mol %)	toluene	70	24	>95
PPh_3 (1 mol %)	toluene	1	18	>95
PPh_3 (1 mol %)	DCM	1	18	0
PPh_3 (1 mol %)	1/1 toluene/MeOH	1	18	0
PPh_3 (1 mol %)	trifluorotoluene	1	18	>95

[a] The percent product conversion was obtained by NMR integration of the product and any starting material remaining and normalizing to 100%. [b] Added as a 48% solution in water.

Table 3. Substrate Scope for the Hydrogenation Precatalyst 1a[a]

Substrate	Product	Pressure (atm)	Conversion (%)[b]
		1 atm	>95% (92%)[c]
		1 atm	>95% (96%)
		1 atm	>95% (97%)
		1 atm	>95%
		1 atm	>95%
		1 atm	94% (83%)
		1 atm	41%
		5 atm	>95% (96%)
		1 atm	46%
		5 atm	>95% (98%)
		1 atm	34%
		5 atm	>95% (85%)
		1 atm	>95%
	-	1 atm	0%

[a] Catalytic conditions: complex 1a (1 mol %), PPh$_3$ (1 mol %), toluene, 35 °C, 18 h. See the Experimental Section for full procedures. [b] The percent product conversion was obtained by NMR integration of product and any starting material remaining and normalizing to 100%. [c] Values in parentheses are isolated yields.

under the mildest conditions reported to date. However, it is remarkable that such a specific ligand set is needed for good hydrogenation activity and that small changes to the ancillary NHC make such a large difference to activity.

Substrate Scope. We were interested in exploring the substrate scope (Table 3). Although room temperature is sufficient for full conversion of the optimization substrate, we found that temperatures of 35 °C are needed for the full conversion of several other compounds, possibly due to the increased solubility of 1a. Several substitutions on the quinoline are permitted, including functionalities at the 2-, 6-, and 8-positions. Homogeneous hydrogenation of quinolines with substitutions at the 8-position is unusual and rarely reported.[9] Halo substituents are also tolerated, and the resulting aryl halide products could potentially be used as substrates for Pd cross-coupling reactions, allowing complex molecules to be rapidly constructed. Higher

pressures of hydrogen (5 atm) improved the yields for less hindered substrates such as quinoline; however, in all cases our pressures are far lower than those typical for this type of homogeneous hydrogenation. Furthermore, the reaction is completely insensitive both to water and to air prior to the addition of hydrogen and, therefore, no special precautions or purifications are required. Unconverted starting material was the sole organic impurity after hydrogenation, and no side products were observed. The imine N-benzylideneaniline can undergo hydrogenation to full conversion under these conditions, while acetophenone is completely unreactive.

Isolation and Observation of Relevant Iridium Hydrides. We were interested in isolating any potential catalytic intermediates with the hope of understanding the mechanism. The neutral meridional iridium trihydride species 2 (Scheme 3) was isolated from a mixture of 1a, PPh$_3$, and H$_2$ in the presence of the
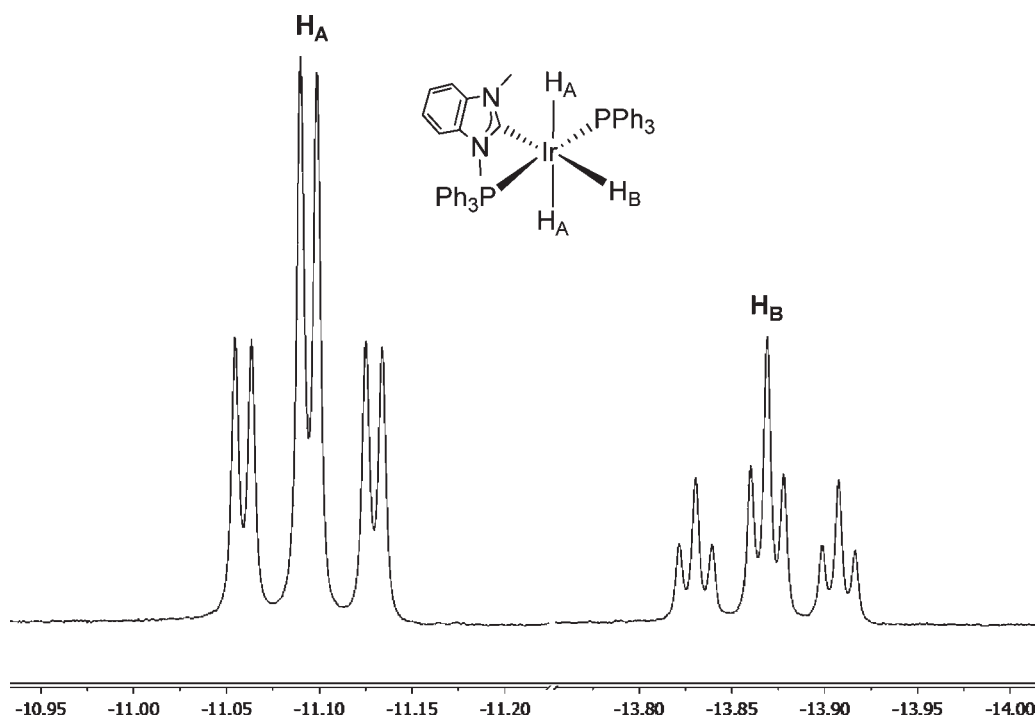
Figure 2. ^{1}H NMR spectrum of the hydride region of **2** (500 MHz NMR, CD$_2$Cl$_2$). Signals and coupling constants: H$_A$, δ −11.08 (td, J_{PH} = 17.6 Hz, J_{HH} = 4.4 Hz, 2H, Ir−H); H$_B$, −13.86 (tt, J_{PH} = 19.3 Hz, J_{HH} = 4.4 Hz, 1H, Ir−H).

Scheme 3. Generation of Trihydride 2 from Catalytic Precursor 1a
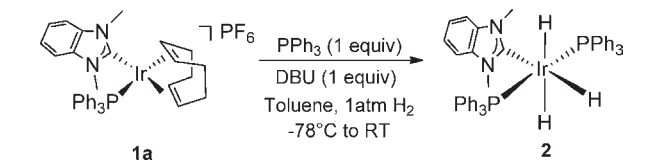
noncoordinating base DBU (1,8-diazabicyclo[5.4.0]undec-7-ene). Although X-ray-quality crystals of **2** could not be obtained, the ^{1}H and ^{31}P NMR chemical shifts and ^{1}H−^{1}H and ^{31}P−^{1}H coupling constants unambiguously confirm the proposed meridional structure. Signals at δ −11.08 and −13.86 ppm (CD$_2$Cl$_2$) integrating to two protons and one proton, respectively, are assigned to two types of hydride (Figure 2). The signal at δ −11.08 ppm is a triplet of doublets (J_{PH} = 17.6 Hz, J_{HH} = 4.4 Hz), while the δ −13.86 resonance is a triplet of triplets (J_{PH} = 19.3 Hz, J_{HH} = 4.4 Hz). The small J_{PH} coupling constants require that all the hydrides be cis to the phosphines, which must also be mutually trans. The coupling assignments were confirmed in the ^{1}H{^{31}P} spectrum, which shows a doublet (δ −11.08) and a triplet (δ −13.86). Only one resonance was observed in the ^{31}P{^{1}H} NMR spectrum, consistent with the PPh$_3$ ligands being mutually trans. On the basis of these data we assign the δ −11.08 signal to the hydrides cis to the NHC and the δ −13.86 signal to the hydride trans to the NHC. Meridional trihydrides of iridium are rare—the *fac* geometry is usually preferred, and only a few *mer* examples have been reported, mostly with tridentate pincer ligands.[29,30]

Addition of 1 equiv of the strong acid [H(Et$_2$O)$_2$][BAr$^F_4$][31] to complex **2** afforded the single species **3a**, which was not isolable
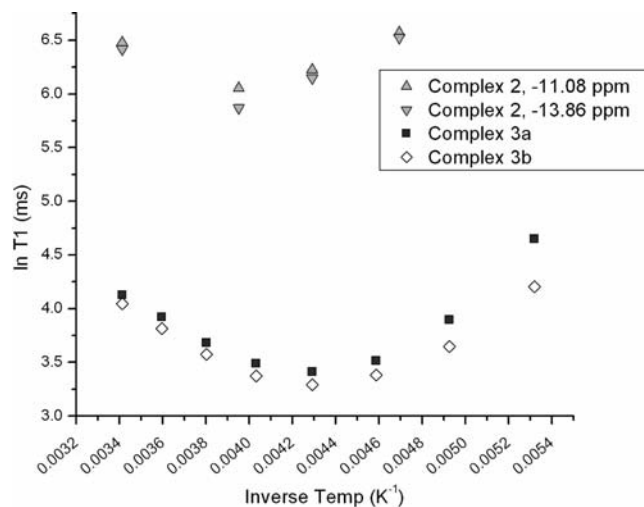
Figure 3. Plot of ln T_1 vs inverse temperature for iridium hydride complexes **2** and **3a,b** at 11.7 T (500 MHz).

Scheme 4. Generation of the Dihydrogen Complex 3a
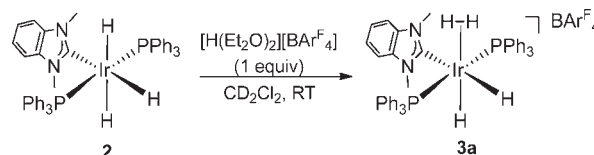
and could only be identified by NMR spectroscopy (Scheme 4). A single broad hydride resonance in the ^{1}H NMR of **3a** at δ −7.71 ppm and corresponding to 4H per Ir shows no

Scheme 5. Formation of the Iridium Dihydride 4 and the Dihydrogen Species 3b
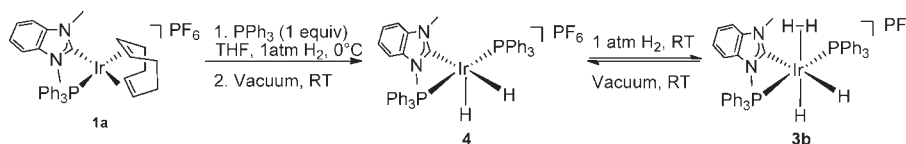
discernible coupling, with no apparent change in line shape from 183 K to 293 K in CD_2Cl_2. The NMR data are consistent with several possible structures. Leading possibilities include a fluxional classical iridium(V) tetrahydride and a fluxional nonclassical iridium(III) dihydrogen dihydride. Combined experimental and computational data discussed below permit a reasonable proposal for the solution structure.[32]

The minimum spin−lattice relaxation time $(T_1(\text{min}))$ of hydride NMR signals with variable temperature is a well-established diagnostic tool for differentiating between classical and nonclassical hydrides.[33] Figure 3 shows the results of inversion recovery experiments for the two hydride signals seen in the ^{1}H NMR spectrum of 2, as well as the single resonance in the spectrum of 3a.

A nonclassical hydride signal typically exhibits a $T_1(\text{min})$ value no larger than 35 ms at 250 MHz.[33] This corresponds to 70 ms at 500 MHz because $T_1(\text{min})$ scales linearly with field strength. The minimum T_1 value seen for complex 3a is 30 ms at 233 K at 500 MHz (CD_2Cl_2). This is in contrast with the minimum value of 350 ms at 253 K for complex 2 (CD_2Cl_2). These values suggest that complex 3a must contain at least one H_2 ligand, while complex 2 only contains classical hydrides. The broad hydride peak in complex 3a can then be assigned to the coalescence of both classical and nonclassical hydrides due to rapid fluxional exchange combined with "anomalous broadening" probably due to ion pairing with the counterion.[34] Although evidence for this fluxional exchange could not be obtained by a variable-temperature NMR experiment, computational studies suggest that the nonclassical and pure tetrahydride isomers are close in energy (vide infra). In addition, in the former isomer, the dihydrogen ligand prefers to be trans to a hydride ligand, as shown in Scheme 4.

A different iridium hydride can be isolated from the reaction of catalyst precursor 1a, PPh₃, and hydrogen in THF, without the need for any base (Scheme 5). During the reaction the orange-red solution becomes colorless as a white solid precipitates. The precipitated white solid readily converts to an orange material on applying a vacuum, presumably owing to loss of hydrogen. This color change is completely reversible under 1 atm of H_2, and the orange color fades to colorless within a few seconds.

X-ray crystallography indicates that this orange material is an ionic iridium hydride, 4 (Figure 4). The PPh₃ ligands are mutually trans, as in the trihydride. The P(1)−Ir(1)−P(2) bond angle is 170.78(7)°, comparable to that observed in other iridium(III) species with trans phosphines. Although the hydrides could not be located in the difference density map, we can infer their presence from charge balance and the ^{1}H NMR spectrum of the complex and the data are consistent with a cis hydride geometry. We have previously reported the X-ray structures of coordinatively saturated trans-bis(triphenylphosphine)iridium(III) NHC complexes which feature cis hydrides.[35]

Efforts to confirm that 4 is a classical iridium(III) dihydride rather than an iridium(I) dihydrogen complex by interpretation
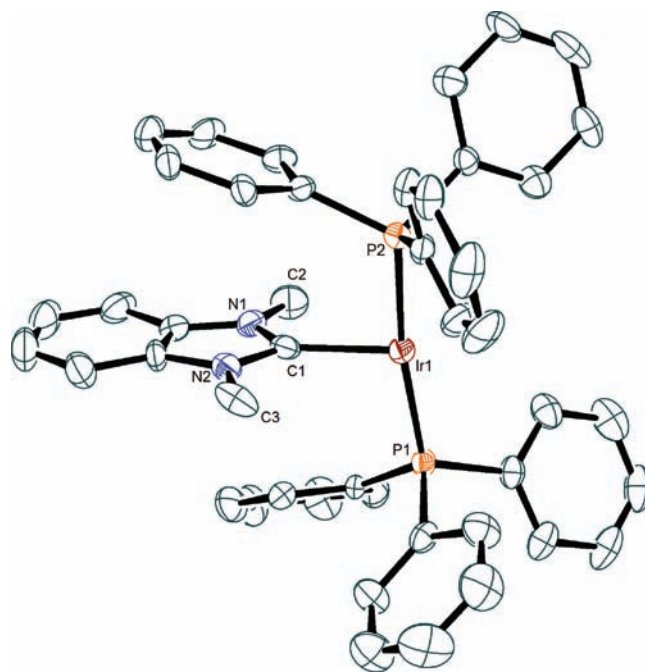
Figure 4. ORTEP representation of 4, as determined by X-ray crystallographic analysis. The PF_6 anion has been removed for clarity. Selected bond lengths (Å) and angles (deg): C(1)−Ir(1) = 2.083(7), N(1)−C-(1) = 1.353(10), N(2)−C(1) = 1.361(10), N(1)−C(2) = 1.448(11), N(2)−C(3) = 1.452(11), Ir(1)−P(2) = 2.315(2), Ir(1)−P(1) = 2.294(2); P(1)−Ir(1)−P(2) = 170.78(7), P(1)−Ir(1)−C(1) = 95.3(2), P(2)−Ir(1)−C(1) = 93.3(2), C(1)−N(2)−C(3) = 123.9(7), C(1)−N(1)−C(2) = 125.6(7), Ir(1)−C(1)−N(1) = 129.8(6), Ir(1)−C(1)−N(2) = 125.1(6).

of T_1 data were complicated by the behavior of the complex at variable temperature (Figure 5). At room temperature a single hydride resonance is present, integrating to two protons. At 188 K, this resonance is absent; instead, two signals can be seen, in a 1:1 intensity ratio, at −11.34 and −18.50 ppm. Both sets of resonances are present at intermediate temperatures. The spectra are inconsistent with normal coalescence, and two species are clearly present at intermediate temperatures. Possible explanations for this behavior are coordination of the anion or of solvent at low temperatures. Treatment of 4 with H_2 forms complex 3b, which shows a broad single hydridic peak at −7.77 ppm, similar to the case for the dihydrogen complex 3a. The $T_1(\text{min})$ value (27 ms at 233 K; Figure 3) confirms that this is an H_2 complex. We therefore suggest that 3b is the PF_6 analogue of 3a. Complex 4 can also be generated by application of vacuum to a sample of dihydrogen complex 3b.

Complex 4 reacts with CD_2Cl_2 over several days to form $[(\text{NHC})(\text{PPh}_3)_2\text{IrHCl}]PF_6$. This is a possible mode of catalyst deactivation in catalytic reactions in dichloromethane, perhaps
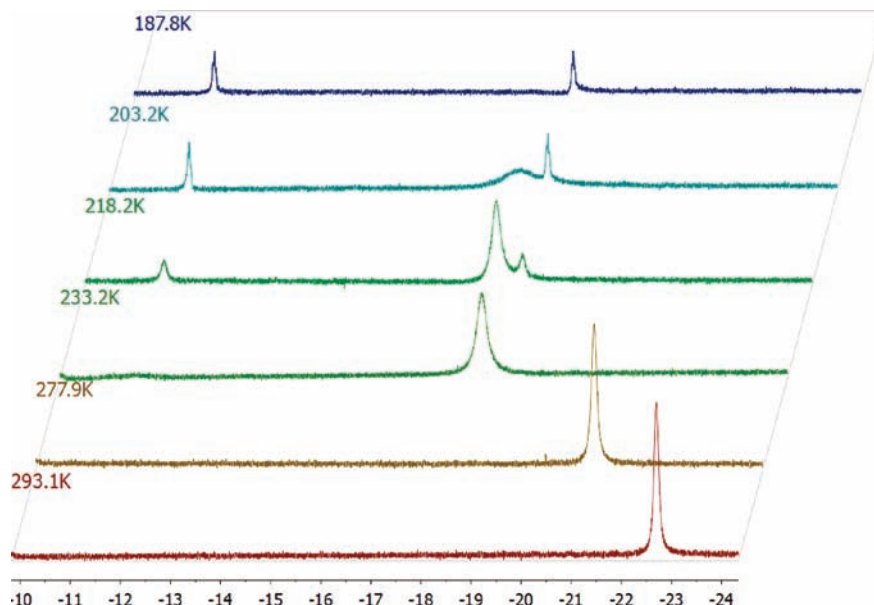
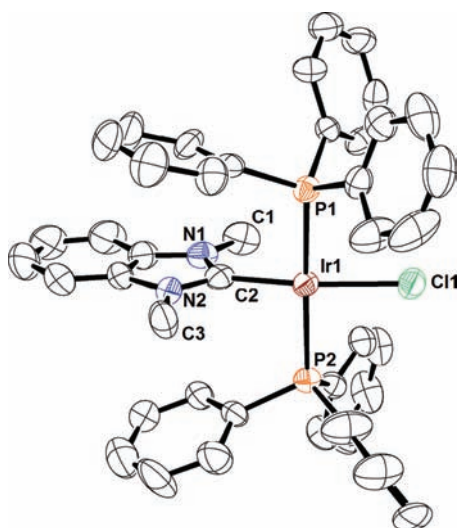**Figure 5.** ^1H NMR spectra of the hydride region of **4** at variable temperatures (500 MHz, CD_2Cl_2).

Figure 6. ORTEP representation of $[(NHC)(PPh_3)_2IrHCl]PF_6$, as determined by X-ray crystallographic analysis. The PF_6 anion has been removed for clarity. Selected bond lengths (Å) and angles (deg): C(2)−Ir(1) = 2.004(8), N(1)−C(1) = 1.468(12), N(2)−C(3) = 1.469(12), N(1)−C(2) = 1.385(10), N(2)−C(2) = 1.360(11), Ir(1)−P(2) = 2.353(2), Ir(1)−P(1) = 2.348(2), Ir(1)−Cl(1) = 2.388(2); P(1)−Ir(1)−P(2) = 173.17(7), P(1)−Ir(1)−C(2) = 91.3(2), P(2)−Ir(1)−C(2) = 91.5(2), C(2)−N(2)−C(3) = 127.5(6), C(2)−N(1)−C(1) = 123.9(7), Ir(1)−C(2)−N(1) = 121.3(6), Ir(1)−C(2)−N(2) = 131.8(6).

explaining the poor conversions seen in that solvent (vide supra). Figure 6 shows that the monohydride complex is square pyramidal with a vacancy trans to H consistent with the high trans influence of H. There is a small decrease in the carbene−Ir bond length upon substitution of H by Cl (2.004(8) Å in the monohydride vs 2.083(7) Å in the dihydride) due to the lower trans influence of chloride versus hydride. The P−Ir bond lengths are approximately 0.05 Å longer in the monohydride. There is a corresponding increase in the P−Ir−P bond angle

(170.78(7)° to 173.17(7)°), bringing that geometry closer to linearity.

Computational Studies of the Iridium Hydrides. To gain further insight into the structure of the neutral complex **2** and the cations of **3a,b** and **4**, we carried out a DFT study on the full system, the only approximation being that the counteranion is not explicitly treated. To reduce the computational cost, QM/MM calculations were performed using the ONIOM (B3PW91:UFF) methodology, including the Ph in the MM part. This level of calculation gives accurate geometries, as illustrated in the present case by comparison with the crystal structures of **4**. Single-point calculations including the solvent effects (toluene) on the optimized structures were then carried out with the M06 functional. These energies are shown in Figure 7 (see Computational Details).

From among all the isomers possible in an octahedral complex with four different ligands, only the four isomers depicted in Figure 7 were considered. The selection is based on the fact that a dihydrogen ligand prefers to be trans to a strong σ donor such as carbene or hydride. Complexes with cis and trans phosphines (**I** used as energy reference, **II** vs **III**, **IV**) were considered, in order to check the preference for the trans phosphines observed experimentally. In each case, we searched for dihydrogen trans to either carbene or hydride. The lowest energy structures correspond to dihydrogen trans to the hydride, **II** (ΔE_{sol} = −6.0 kcal mol^{-1}) and **IV** (ΔE_{sol} = −6.4 kcal mol^{-1}), which is the ligand with the largest trans influence. Of these two structures, the isomer with trans phosphines, **IV**, is more stable.

The relative trans influence of hydride and NHC also accounts for the change in H···H distance of the coordinated H_2 ligand depending on the isomer considered. The higher trans influence of the hydride is responsible for the shorter H−H bond (0.86 Å trans to H in **II**, vs 0.88 Å trans to NHC in **III**). The long Ir−C(NHC) distance of 2.15 Å in **III** decreases the trans influence of this ligand. This, in turn, elongates the H···H distance in **III**, which is best considered as an Ir(V) tetrahydride complex.

The energetic preference for isomer **IV** is consistent with the experimental structure of the cation of **3a**. In addition, the broad
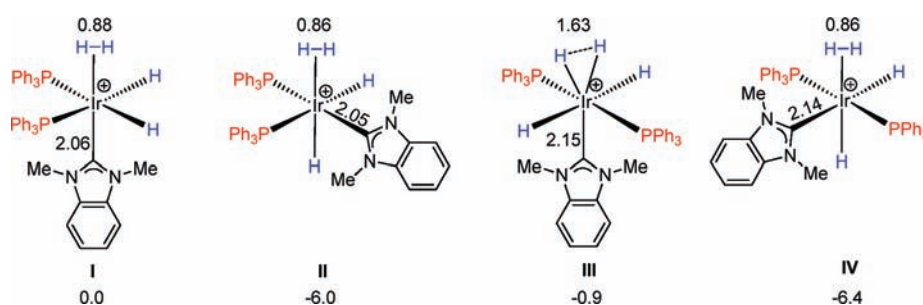
Figure 7. Isomers considered for the cation of **3a** or **3b**, with selected distances in Å. Energies are in kcal mol^{-1} relative to **I**.
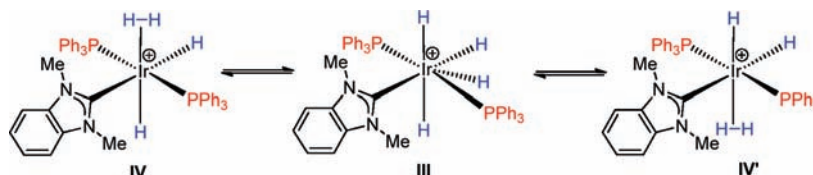
Figure 8. Equilibrium proposed on the basis of the observed NMR data of **3a,b**.
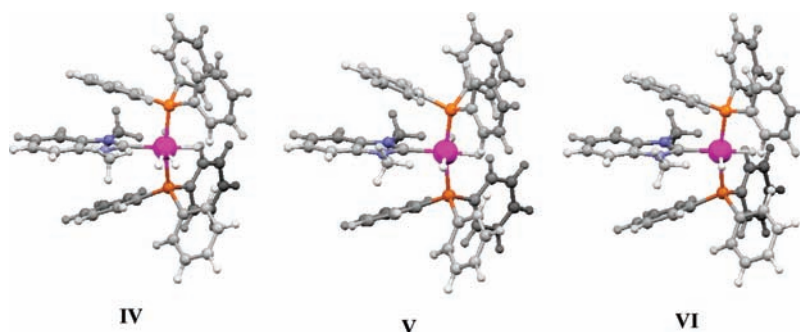
Figure 9. Optimized structures of the cationic dihydrogen dihydride **IV**, the neutral trihydride **V**, and the cationic dihydride **VI**.

hydride peak in the NMR spectrum of **3a** could be explained by a fast exchange between **IV** and **IV′** going through a higher energy intermediate **III** (Figure 8).

The *mer* geometry of **V** (Figure 9) is consistent with the NMR data obtained for trihydride **2** (vide supra). Hexacoordinated Ir(III) trihydrides have an intrinsic preference for a *fac* geometry to avoid hydrides to be mutually trans. However, they tend to be *mer* when encouraged to do so by the accompanying ligands. This happens with a pincer ligand[30] or, as in **2**, in the presence of two bulky phosphines that prefer to be trans.[36] Upon protonation to give the nonclassical tetrahydride **3a**, we expect the H ligand trans to another H to be the most basic and thus most easily protonated. The geometrical features follow the relative basicity, since the Ir–H bond is longer when trans to H (1.66 Å) than to NHC (1.63 Å). The dihydrogen dihydride product **IV** retains the structure of **V**, having H$_2$ trans to H (Figure 9).

The energy to dissociate H$_2$ from complex **IV** has been evaluated in the full system as 11.0 kcal mol^{-1}. This is consistent with the facile H$_2$ elimination from complexes **3a,b**. Upon loss of H$_2$, the dihydride complex, **VI** in Figure 9, has a square-based-pyramidal structure with an apical hydride trans to the empty coordination site. The Ir–H bond trans to the empty coordination is shorter than that trans to NHC (1.53 Å vs 1.63 Å).

Scheme 7. Attempted Catalysis Using Isolated Iridium Species as Catalytic Precursors
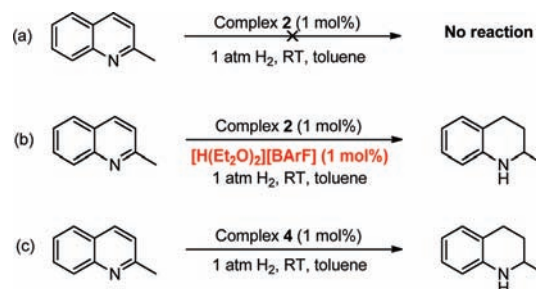
Reactivity of Isolated Iridium Hydrides in Hydrogenation Reaction. We evaluated the catalytic competence of the isolated iridium hydride complexes to establish whether they were potential intermediates in the catalytic cycle (Scheme 7). Trihydride **2** failed to hydrogenate 2-methylquinoline under our previously optimized conditions, suggesting the neutral complex is not a competent precatalyst (Scheme 7a). However, catalytic hydrogenation of 2-methylquinoline to the tetrahydro form became possible when [H(Et$_2$O)$_2$][BAr$^F_4$] was added to

Scheme 8
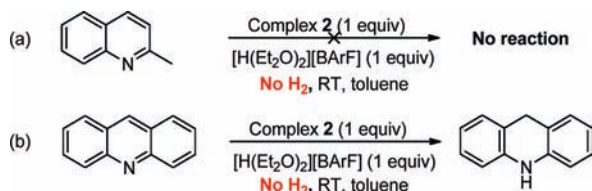
complex **2** (1:1 acid:complex, 1 mol % loading) (Scheme 7b). Most likely, prior protonation of substrate allows for hydride delivery from **2**. Unlike complex **2**, dihydride **4** is competent for catalytic quinoline hydrogenation in the absence of acid (Scheme 7c). Since we have observed the formation of a dihydrogen complex upon exposure of **4** to hydrogen, we surmise that a dihydrogen complex analogous to **3a** is formed in situ and that this acidic species is then capable of stepwise proton delivery and hydride delivery to substrate.

If **3a** is capable of sequential proton transfer/hydride transfer, it should also be capable of stoichiometric reduction of C=N double bonds in the absence of hydrogen. To check this point, **3a** was generated in situ by combining **2** and $[H(Et_2O)_2][BAr^F_4]$ in a 1:1 mixture, and 1 equiv of 2-methylquinoline was added. In the absence of hydrogen, no reaction occurred (Scheme 8a), but upon addition of hydrogen, the reduction product appeared. In contrast to 2-methylquinoline, acridine can be reduced *in the absence of hydrogen gas* by a 1:1 mixture of **2** and $[H(Et_2O)_2][BAr^F_4]$ (Scheme 8b). 9,10-Dihydroacridine was observed in the ^1H NMR spectrum of a 1:1:1 mixture of complex **2**, acridine, and $[H(Et_2O)_2][BAr^F_4]$. Additionally, the formation of complex **4** is indicated in the ^1H NMR spectrum by the presence of a hydride resonance at δ −22.19 ppm. Successful reduction in the absence of hydrogen, coupled with the formation of complex **4**, strongly suggests that **3a** has a role in the catalytic hydrogenation reaction. Acridine may react because it only requires 2H to achieve a stable final product, while quinolines require 4H. A 1,4-hydride/proton addition would not be expected to occur as easily as a 1,2-addition if the reaction were concerted. The easy reduction of acridine, presumably by a 1,4-addition, is thus consistent with a stepwise process.

Computational Studies on the Hydrogenation Mechanism. Two main classes of mechanism have been proposed for the hydrogenation of heteroaromatic substrates: an inner-sphere mechanism (Scheme 9a) and an outer-sphere mechanism where the proton and the hydride could be transferred in a concerted manner or in two separate steps (Scheme 9b).[16] However, it is difficult to choose between them on the basis of experiments

alone for the present system. Thus, even though the 18e trihydride can only directly participate in a stepwise outer-sphere mechanism, it could be protonated and deliver H_2 to give a 16e cationic dihydride that could give an inner-sphere reaction. Consequently, we evaluated the preference between the outer- and the inner-sphere mechanisms by DFT calculations. These calculations were carried out modeling the phosphine ligand by PH_3 and the experimental carbene by $C_2H_2(NMe)_2C$. The energy profiles using this model were sufficiently distinct to demonstrate that the inner-sphere mechanism is unlikely for this catalyst. The energies reported are Gibbs energies with solvent (toluene) effects, and the units are kcal mol^{-1} (see Computational Details). All Gibbs energies are given at 25 °C relative to separated species, the dihydrogen dihydride model for the cation of **3a** and 2-methylquinoline. The activation barrier is defined as the difference in Gibbs energy between a transition state and its associated reactants.

Our labeling for the model system is as follows: the organometallic complexes are labeled by the nature of the ligand trans to the apical hydride of the 16e$^-$ dihydride complex, labeled as [**0**]. The trihydride is labeled as [**H**] and the dihydrogen dihydride complex as [**H$_2$**]. The labels **A**–**D** are used for the organic species: **A** is the unprotonated quinoline, **B** the monoprotonated species, **C**$_{xy}$ for the dihydrogenated form with H atoms in positions x and y, **D** for the trihydrogenated product, and **E** for the tetrahydrogenated product. Finally labels such as [**H$_2$-H**]$^{\ddagger}_{AB}$ denote transition states (TS); for instance, [**H$_2$-H**]$^{\ddagger}_{AB}$ is the TS in which [**H$_2$**] hydrogenates **A** into **B** and turns itself into [**H**].

The inner-sphere mechanism starts by the decoordination of H_2 to generate a vacant site at Ir (Figure 10). From the dihydrogen complex, [**H$_2$**], this process has an energy cost of 9.2 kcal mol^{-1}. After this dissociation, the quinoline insertion to the basal Ir–H bond of the square pyramid has an activation barrier of 41.2 kcal mol^{-1}. In addition to the large energy barrier, this process is endoergic by 23.3 kcal mol^{-1}. This mechanism is clearly unfavorable even for PH_3; thus, there is little need to consider the same process with the real phosphines since the steric influence of these ligands should not make this process more favorable.

A concerted outer-sphere mechanism, where a proton from the dihydrogen ligand and the hydride are simultaneously transferred to the N=C bond of the quinoline, could not be located. Instead we found that the two H transfers occur via separate transition states, as represented in Figures 11 and 12. Figure 11 shows the energy profile for the first H_2 addition to quinoline **A**, while Figure 12 shows the second H_2 addition to dihydroquinoline **C$_{34}$**. Note that in both profiles the

Scheme 9. Two Mechanistic Proposals for the Hydrogenation of Quinoline: (a) Inner-Sphere Hydrogenation Mechanism; (b) Stepwise Outer-Sphere Mechanism
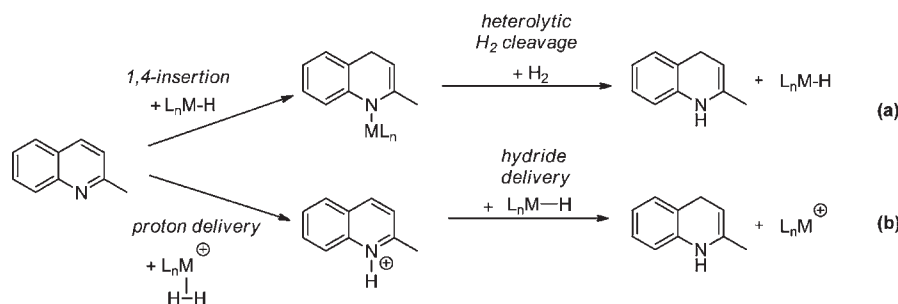
Figure 10. Gibbs energy profile, ΔG, in kcal mol^{-1}, for the inner-sphere hydrogenation pathway.

Figure 11. Gibbs energy profile, ΔG, in kcal mol^{-1}, for the first outer-sphere hydrogenation of 2-methylquinoline.

Figure 12. Gibbs energy profile, ΔG, in kcal mol^{-1}, for the second outer-sphere hydrogenation of 2-methylquinoline.

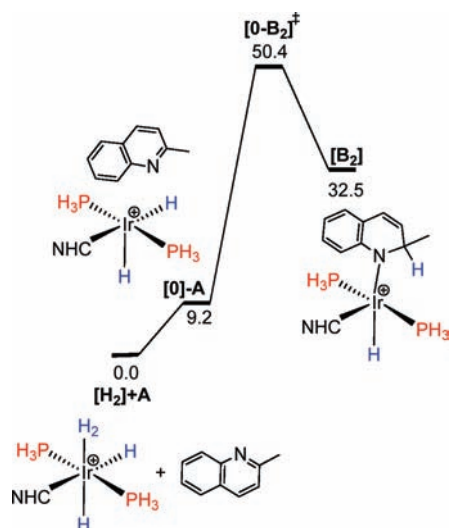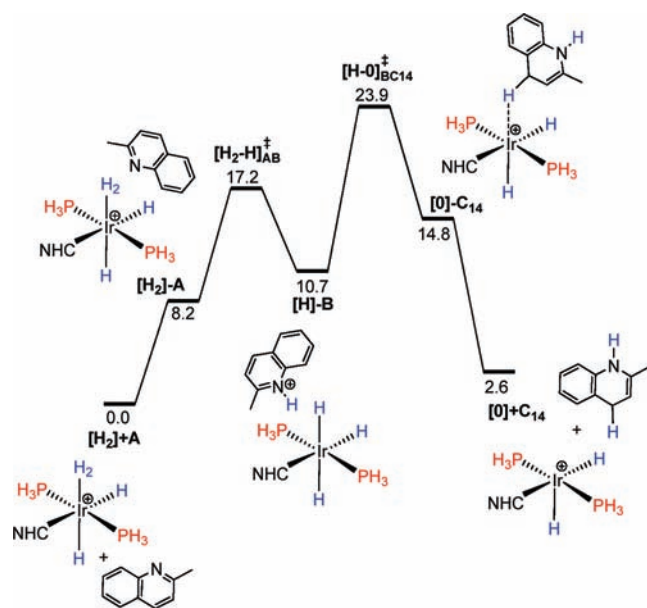organometallic complexes are the same ($[\mathbf{H2}] \rightarrow [\mathbf{H}] \rightarrow [\mathbf{0}]$); therefore, the difference in energy in those cases comes from the organic fragment.

The first hydrogen transfer from $[\mathbf{H_2}]$ to $\mathbf{A}$ starts with proton migration from the dihydrogen ligand to the N of the quinoline. The transition state for this H transfer is 17.2 kcal mol^{-1} above the isolated reactants: 8.2 kcal mol^{-1} of this energy is used to form the ion pair $[\mathbf{H_2}]$-$\mathbf{A}$ and 9.0 kcal mol^{-1} for the proton transfer. This reaction is slightly endoergic, with the product $[\mathbf{H}]$-$\mathbf{B}$ being 2.5 kcal mol^{-1} above $[\mathbf{H_2}]$-$\mathbf{A}$. Once $\mathbf{A}$ is protonated, positions 2 and 4 are activated for the subsequent hydride transfer. Both possibilities have been considered, and the energies for the transition states $[\mathbf{H}\text{-}\mathbf{0}]^{\ddagger}_{BC12}$ and $[\mathbf{H}\text{-}\mathbf{0}]^{\ddagger}_{BC14}$ are $\Delta G^{\ddagger} = 26.3$ and 23.9 kcal mol^{-1}, respectively. Figure 12 shows the second possibility, which has the lowest energy barrier. From

$[\mathbf{H}]$-$\mathbf{B}$, the hydride transfer is endoergic by 4.1 kcal mol^{-1}. Further reaction of $[\mathbf{0}]$ with dihydrogen is thus needed to complete an exergonic process. This could explain why **3a** does not react experimentally with 2-methylquinoline and acid in the absence of H$_2$.

As shown in Figure 11, the formation of $[\mathbf{0}] + \mathbf{C_{14}}$ is endoergic by 2.6 kcal mol^{-1}, relative to the initial reactants, $[\mathbf{H_2}]$+$\mathbf{A}$, although isomerization of $\mathbf{C_{14}}$ to $\mathbf{C_{34}}$ stabilizes this species by 1.5 kcal mol^{-1} (not shown in Figure 11). The hydrogenations of $\mathbf{C_{14}}$ and $\mathbf{C_{34}}$ by $[\mathbf{H_2}]$ have significantly different energy profiles. In the case of $\mathbf{C_{14}}$, complex $[\mathbf{H_2}]$ can only protonate the carbon in the 3-position; this step has a transition state with a Gibbs energy of 24.5 kcal mol^{-1}. For $\mathbf{C_{34}}$, this protonation takes place at the nitrogen and is energetically more favorable, with a transition state at 16.2 kcal mol^{-1} (Figure 12). In both cases, the protonation yields the ion pair $[\mathbf{H}]$-$\mathbf{D}$, with a Gibbs energy of 10.0 kcal mol^{-1}. The transition state for the hydride transfer to the 2 position has a Gibbs energy of 23.5 kcal mol^{-1}, which is very similar to that of the TS for the first hydride transfer ($\Delta G^{\ddagger} = 23.9$ kcal mol^{-1}). This process leads to the final product, with a favorable Gibbs energy of 7.7 kcal mol^{-1}.

These computational results suggest that a stepwise outer-sphere pathway is the most likely mechanism of hydrogenation (Scheme 10). A cationic iridium H$_2$ complex first gives proton transfer to substrate, resulting in a neutral species and a protonated substrate. Hydride transfer to the substrate in a later step results in the formation of a coordinatively unsaturated, cationic metal center, which then coordinates hydrogen and completes the catalytic cycle. Isomerization of dihydroquinoline can take place with classical acid catalysis in the presence of protons liberated by the acidic iridium dihydrogen complex, thus allowing for the dihydro form to undergo subsequent hydrogenation to the tetrahydroquinoline. In our experimental work we have isolated or spectroscopically characterized all of the proposed intermediates, which provides strong support for this mechanism. Furthermore, in stoichiometric reactions we have demonstrated that each of the intermediates can perform the reactions we propose in our mechanism; the molecular hydrogen species

Scheme 10. Proposed Stepwise Outer-Sphere Mechanism for the Hydrogenation of Quinolines
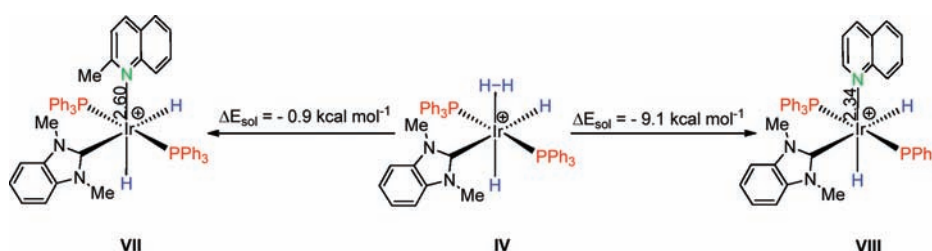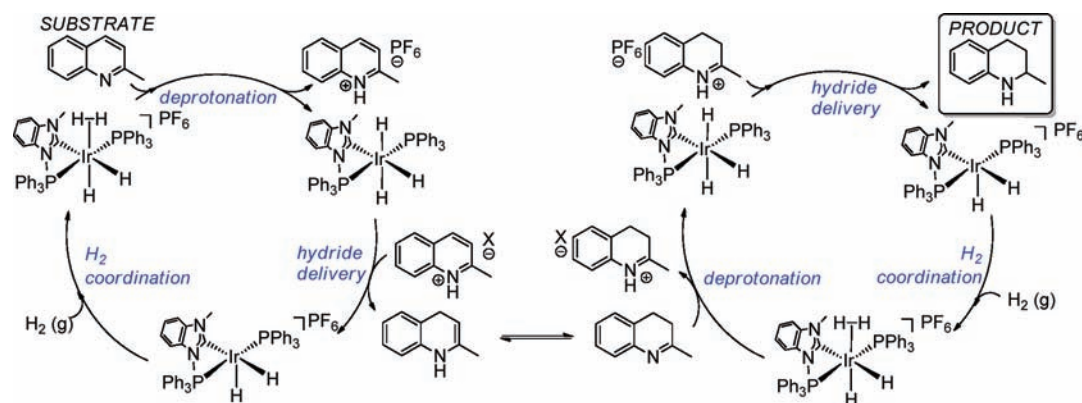
Figure 13. Relative energies of complexes with coordinated quinoline and 2-methylquinoline.

can be deprotonated by base, the trihydride can deliver a hydride, and the resulting coordinatively unsaturated species can bind dihydrogen.

Implications of Mechanistic Studies for Catalysis. The mechanistic results provide a rationale for several observations made during the original screening. Additional triphenylphosphine is presumably required to form the intermediate iridium hydride complexes that are responsible for catalysis, while the comparatively small N-methyl wingtip groups on the NHC allow for the coordination of two phosphines. The noncoordinating PF_6 anion also allows the dihydride to remain coordinatively unsaturated so that it may react with free hydrogen. This may be an advantage over previous iridium catalysts, which feature coordinating halides that may inhibit the formation of the active catalyst or slow the rate of the hydrogenation by competing for a coordination site.

Though proposals for a stepwise outer-sphere reaction mechanism are unusual and are not often considered, it is possible that prior quinoline hydrogenation catalysts, in particular those with $[Ir(cod)Cl]_2$ as precursor,[9−14] could function by this type of mechanism. The considerable steric bulk of the chiral bisphosphines employed in many asymmetric quinoline hydrogenations, coupled with the steric demand of the hindered substrates typically used, could make inner-sphere substrate coordination unfavorable. Furthermore, acid increases the rate of reaction in several of these hydrogenations[11,18] and the acid may have a role in proton transfer. Acid presumably prevents coordination of a substrate's nitrogen lone pair due to protonation. It is noteworthy that several systems contain I_2 as an additive. Under the reaction conditions I_2 could plausibly react with metal hydrides formed during the hydrogenation reaction to generate hydroiodic acid.

The high energy barrier for the inner-sphere hydrogenation of quinoline may be due to its aromaticity. The high-lying empty π^*

orbitals of quinoline cannot efficiently stabilize the hydride in the insertion step, even with the assistance of the metal. In contrast, in the two-step mechanisms, the protonation of the quinoline decreases its aromaticity and significantly lowers the energy of its empty π^* orbitals. The hydride addition is thus facilitated. Direct π-binding of aromatic substrates to the metal may also be disfavored by steric effects relative to the outer-sphere route. These points may well apply to other aromatic hydrogenation catalysts and make the outer-sphere hydrogenation process the path of choice.

The substrate selectivity may be partially limited by pK_a differences between proton donor (the dihydrogen complex) and proton acceptor (substrates). Ketones are not as basic as quinolines, and this decrease in basicity may make substrate protonation relatively unfavorable. An increase in the acidity of the H_2 complex may allow for the hydrogenation of these classes of substrates. Chan et al., who invoke a stepwise outer-sphere mechanism for their quinoline hydrogenation reaction, report that their system preferentially performs C=N hydrogenation over C=O hydrogenation.[8]

Steric effects may also be responsible for defining the substrate scope. Hydrogenation of nitrogen heterocycles is most efficient with 2-methylquinoline and derivatives with other substituents at the same position. Remarkably, catalytic efficiency falls for quinoline itself and other less hindered substrates such as ketones. The proposed mechanism absolutely requires H_2 coordination to the metal center to allow protonation of the substrate. This coordination is not possible if the substrate is a better ligand than H_2. This explains the failure of the reaction with a variety of sterically unhindered nitrogen- and oxygen-containing substrates. With bulky substrates, coordination is prevented and the binding of H_2 is allowed. To quantify this

effect, the energy required to replace H_2 with 2-methylquinoline or quinoline has been computed (Figure 13). This shows that substitution of H_2 by the former substrate is almost thermoneutral (**IV** → **VII**, $\Delta E_{sol} = -0.9$ kcal mol^{-1}), while the latter is thermodynamically favorable (**IV** → **VIII**, $\Delta E_{sol} = -9.1$ kcal mol^{-1}), in agreement with our hypothesis.

The inability of hindered substrates to compete with hydrogen gas for coordination is a result of the considerable steric demand of the triphenylphosphine ligands. The excellent conversions obtained in the quinoline hydrogenation reaction with the appropriate ligand set demonstrate that the optimal ligands are bulky enough to prevent substrate coordination yet not bulky enough to prevent two phosphines from maintaining coordination. This specific steric requirement may explain the narrow range of ligands, which demonstrate activity for the reaction.

■ CONCLUSIONS

We report an unusually mild homogeneous hydrogenation of N-heterocycles at low pressures of hydrogen. Our air-stable precursors and the low pressures required for reactivity allow for the reaction to be performed without exhaustive purification or special handling. The catalysts are selective for C=N bonds over C=O bonds and tolerant of halide functional groups, which could make them suitable for practical applications. Mechanistic studies were performed using both computational and experimental techniques. DFT calculations showed that the classical inner-sphere mechanism in which the substrate coordinates to the metal and inserts into a metal–hydride bond is not energetically accessible for these complexes. Instead, the full hydrogenation of the N-heterocycle occurs in a remarkable succession of outer-sphere hydrogenation events, involving a proton transfer from a coordinated acidic dihydrogen ligand, followed by hydride transfer from the resulting classical hydride. The key species was found to be a dihydrogen dihydride complex. Each of the proposed intermediates in our catalytic cycle was either isolated or spectroscopically characterized, and a series of stoichiometric reactions confirmed their role in the catalytic cycle. We believe that preferential binding of H_2 to the metal center over substrate is a crucial factor for the outer-sphere mechanism, and this may explain why the catalyst is highly sensitive to the nature of the ligands in the coordination sphere. It also accounts for the easier hydrogenation of more hindered substrates. Although we have only unambiguously established the stepwise mechanism in this case, we believe that observed results in other hydrogenation systems are consistent with our proposal. Thus, our results could lead to the development of asymmetric catalysts that perform under far milder conditions than existing systems and direct future catalyst design.

■ EXPERIMENTAL SECTION

General Considerations. The syntheses of the ligand precursors and the metal complexes were conducted under nitrogen using dry degassed solvents, unless otherwise indicated. Solvents were dried and degassed prior to use. $[Ir(cod)Cl]_2$,[37] NaBAr$^F_4$,[38] and $[H(Et_2O)_2][BAr^F_4]$[31] were prepared according to literature procedures. $[\eta^4$-1,5-Cyclooctadiene]-[triphenylphosphine](N,N-dimethylimidazol-2-ylidene)iridium hexafluorophosphate (**1d**) was prepared according to the procedure by Buriak et al.[23] $[\eta^4$-1,5-Cyclooctadiene][triphenylphosphine](N,N-bis(2,4,6-trimethylphenyl)imidazol-2-ylidene)iridium hexafluorophosphate (**1f**) was prepared according to the procedure of Nilsson et al.[27] 2-Ethylquinoline and 2-butylquinoline were synthesized using established procedures.[39] All other reagents were commercially available from Sigma-Aldrich, Alfa-Aesar, and Strem Chemicals and used as received unless otherwise indicated. NMR

spectra were recorded at room temperature on a 400 or 500 MHz Bruker or Varian spectrometer and referenced to the residual solvent peak (δ in ppm and J in Hz). High-pressure hydrogen gas reactions were performed using a reactor vessel and a glass sleeve from Parr Instrument Co. (Moline, IL). IR spectra were obtained using a Nicolet 6700 FT-IR spectrometer. Elemental analyses were performed by Robertson Microlit Laboratories (Madison, NJ).

Iodo[η^4-1,5-cyclooctadiene](N,N-dimethylbenzimidazol-2-ylidene)iridium.[40] To a flame-dried Schlenk was added $[Ir(cod)Cl]_2$ (778.3 mg, 1.158 mmol). The flask was evacuated and back-filled with nitrogen. A degassed 1:1 mixture of dichloromethane (20 mL) and tetrahydrofuran (20 mL) was added via syringe. Under a positive flow of nitrogen gas potassium *tert*-butoxide (259.4 mg, 2.316 mmol) was added to the flask. The reaction mixture became a red-brown solution after stirring for 1 h, at which point N,N'-dimethylbenzimidazolium iodide[41] (634.7 mg, 2.316 mmol) was added to the flask under positive flow of nitrogen gas. The reaction mixture was stirred for 4 h. The solvent was removed by rotary evaporation. The residual brown solid was purified by silica gel chromatography (CH$_2$Cl$_2$ eluent, under air) to provide a brown solid (1.26 g, 94% yield). The isolated material was spectroscopically identical with that reported previously.[40]

Bromo[η^4-1,5-cyclooctadiene](N,N-di-n-butylbenzimidazol-2-ylidene)iridium. This compound was synthesized following the above procedure using $[Ir(cod)Cl]_2$ (160.3 mg, 0.239 mmol), potassium *tert*-butoxide (53.4 mg, 0.477 mmol), and N,N'-di-n-butylbenzimidazolium bromide[42] (157.0 mg, 0.477 mmol). The reaction mixture was stirred for 24 h. The solvent was removed by rotary evaporation and purified by silica gel chromatography (CH$_2$Cl$_2$ eluent, under air) to afford a yellow solid (198 mg, 66% yield). ^{1}H NMR (500 MHz, CD$_2$Cl$_2$): δ 7.25 (m, 2H, arene CH), 7.15 (m, 2H, arene CH), 4.70–4.42 (m, 6H, –NCH$_2$C–, COD CH), 2.92 (m, 2H, COD CH), 2.20–2.10 (m, 4H), 2.05–1.95 (m, 2H), 1.83–1.69 (m, 4H), 1.59–1.41 (m, 4H), 0.97 (t, J = 7.4, 3H). ^{13}C{^{1}H} NMR (126 MHz, CD$_2$Cl$_2$): δ 191.93, 135.53, 122.66, 110.67, 85.73, 53.66, 48.62, 33.85, 31.92, 30.22, 20.97, 14.15. Anal. Calcd for C$_{23}$H$_{34}$BrIrN$_2$: C, 45.24; H, 5.61; N, 4.59. Found: C, 45.58; H, 5.55; N, 4.51.

[η^4-1,5-Cyclooctadiene][triphenylphosphine](N,N-dimethylbenzimidazol-2-ylidene)iridium Hexafluorophosphate (1a). In a round-bottom flask was added iodo[η^4-1,5-cyclooctadiene](N,N-dimethylbenzimidazol-2-ylidene)iridium (1260 mg, 2.195 mmol), PPh$_3$ (575 mg, 2.195 mmol), and KPF$_6$ (404 mg, 2.195 mmol). Tetrahydrofuran (5 mL) was added to the flask under air, resulting in a red-orange solution. Additional PPh$_3$ and KPF$_6$ can be added to shorten the required reaction time. After 16 h the solvent was removed in vacuo and dichloromethane was added into the flask. The reaction mixture was washed three times with water in a separatory funnel under air. The organic layer was dried over magnesium sulfate, filtered, and evaporated, leaving a red residue. Fifteen milliliters of dichloromethane was added to the residue, and red solid was precipitated by the addition of 150 mL of diethyl ether. After it stood for 1 h at −20 °C, the suspension was filtered. The solid was rinsed with diethyl ether and dried at 40 °C for 16 h under vacuum over P$_2$O$_5$ to provide the anhydrous red solid product (1477 mg, 76% yield). Crystals suitable for X-ray diffraction were obtained by recrystallizing the material in dichloromethane/diethyl ether. ^{1}H NMR (400 MHz, CDCl$_3$): δ 7.34–7.10 (m, 19H, PPh$_3$, NHC –CH–), 4.41 (m, 2H, cod CH), 3.90 (m, 2H, cod CH), 3.68 (s, 6H, N–CH$_3$), 2.37 (m, 4H, cod CH$_2$), 2.06 (m, 4H, cod CH$_2$). ^{13}C{^{1}H} NMR (125 MHz, CDCl$_3$): δ 186.43, 135.24, 133.57 (d, J = 10.9), 131.21 (d, J = 2.0), 129.95 (d, J = 51.2), 128.86 (d, J = 10.2), 123.35, 109.85, 86.60 (d, J = 11.5), 82.48, 34.71, 31.19, 30.64 (d, J = 2.9). ^{31}P{^{1}H} NMR (162 MHz, CDCl$_3$): δ 17.42 (s), −143.93 (hept, J = 714.2). Anal. Calcd for C$_{35}$H$_{37}$F$_6$IrN$_2$P$_2$: C, 49.23; H, 4.37; N, 3.28. Found: C, 49.16; H, 4.16; N, 3.00.

[η^4-1,5-Cyclooctadiene][triphenylphosphine](N,N-dimethylbenzimidazol-2-ylidene)iridium Tetrakis[3,5-bis(trifluoromethyl)phenyl]borate (1b). In a flame-dried Schlenk flask was added iodo[η^4-1,5-cyclooctadiene](N,N-dimethylbenzimidazol-2-ylidene)iridium (161.9 mg,

0.282 mmol), PPh$_3$ (73.8 mg, 0.282 mmol), and anhydrous NaBAr$^F_4$ (250.0 mg, 0.282 mmol). Dried tetrahydrofuran (5 mL) was added to the flask, resulting in a red-orange solution. The reaction mixture was stirred for 1 h. The solvent was removed in vacuo, and dichloromethane was added into the flask. The reaction mixture was filtered through Celite in vacuo and the solvent was evaporated to afford an orange solid (430 mg, 97% yield). ^{1}H NMR (500 MHz, CDCl$_3$): δ 8.02−7.04 (m, 31H, aromatic), 4.40 (m, 2H, cod CH), 4.03 (m, 2H, cod CH), 3.66 (s, 6H, N−CH$_3$), 2.55−2.01 (m, 8H, cod CH$_2$). ^{13}C{^{1}H} NMR (126 MHz, CDCl$_3$): δ 186.22 (d, J = 9.6 Hz), 161.59 (q, J = 49.9 Hz), 134.98, 134.70, 133.28 (d, J = 10.9 Hz), 131.41, 129.73, 129.32, 129.22−128.34 (q, J = 31.3 Hz), 128.77 (d, J = 10.2 Hz), 127.69, 121.19, 117.36, 109.49, 85.87 (d, J = 11.7 Hz), 82.85, 33.89, 31.01, 30.49. ^{31}P{^{1}H} NMR (202 MHz, CDCl$_3$): δ 17.62. Anal. Calcd for C$_{67}$H$_{49}$BF$_{24}$IrN$_2$P: C, 51.19; H, 3.14; N, 1.78. Found: C, 51.09; H, 2.90; N, 1.81.

[$η^4$-1,5-Cyclooctadiene][triphenylphosphine](_N,N_-di-_n_-butyl-benzimidazol-2-ylidene)iridium Hexafluorophosphate (1c). In a flask was added bromo[$η^4$-1,5-cyclooctadiene](_N,N_-di-_n_-butylbenzimidazol-2-ylidene)iridium (60.0 mg, 0.0952 mmol), PPh$_3$ (25.0 mg, 0.0952 mmol), and KPF$_6$ (17.5 mg, 0.0952 mmol). Dried tetrahydrofuran was added into the flask, and the reaction mixture was stirred for 16 h. The solvent was removed in vacuo, and dichloromethane was added to the flask. The reaction was filtered through Celite under air, and the solvent was removed. The resulting orange solid was purified via recrystallization (dichloromethane/diethyl ether) to afford an orange solid (77 mg, 86% yield). ^{1}H NMR (500 MHz, CD$_2$Cl$_2$) δ 7.49−7.38 (m, 3H, PPh$_3$), 7.35−7.19 (m, 16H, PPh$_3$, NHC −CH−), 4.63−4.49 (m, 4H, cod CH, N−CH$_2$), 3.95 (m, 2H, cod CH), 3.73 (m, 2H, N−CH$_2$−), 2.43−2.30 (m, 4H, cod CH$_2$), 2.28−2.08 (m, 4H, cod CH$_2$), 1.70−1.58 (m, 4H, −CH$_2$−), 1.54−1.43 (m, 4H, −CH$_2$−), 0.99 (t, J = 7.4 Hz, 6H, −CH$_3$). ^{13}C{^{1}H} NMR (126 MHz, CD$_2$Cl$_2$): δ 185.52 (d, J = 9.4 Hz), 135.51, 134.16 (d, J = 10.7 Hz), 131.99 (d, J = 2.2 Hz), 130.26 (d, J = 51.2 Hz), 129.43 (d, J = 10.1 Hz), 123.97, 111.46, 86.90 (d, J = 11.8 Hz), 82.76, 49.78, 31.74 (d, J = 1.9 Hz), 31.39, 31.06 (d, J = 3.1 Hz), 21.12, 14.01. ^{31}P{^{1}H} NMR (202 MHz, CD$_2$Cl$_2$): δ 17.57, −144.56 (hept, J = 709.0). Anal. Calcd for C$_{41}$H$_{49}$F$_6$IrN$_2$P$_2$: C, 52.50; H, 5.27; N, 2.99. Found: C, 52.53; H, 5.22; N, 2.98.

[$η^4$-1,5-Cyclooctadiene][triphenylphosphine](_N,N_-diisopro-pylimidazol-2-ylidene)iridium Hexafluorophosphate (1e). In a flask was added chloro[$η^4$-1,5-cyclooctadiene](_N,N_-diisopropylimidazol-2-ylidene)iridium[43] (43.1 mg, 0.0848 mmol), PPh$_3$ (22.2 mg, 0.0848 mmol), and KPF$_6$ (15.6 mg, 0.0848 mmol). Dried tetrahydrofuran was added into the flask, and the reaction mixture was stirred for 16 h. The solvent was removed in vacuo, and dichloromethane was added into the flask. The reaction mixture was filtered through Celite under air, and the solvent was removed. The resulting orange solid was purified via recrystallization (dichloromethane/diethyl ether) to afford an orange solid (68 mg, 93% yield). ^{1}H NMR (500 MHz, CD$_2$Cl$_2$): δ 7.52−7.46 (m, 3H, PPh$_3$), 7.41 (td, J = 7.6, 2.2 Hz, 6H, PPh$_3$), 7.21−7.13 (m, 6H, PPh$_3$), 7.11 (s, 2H, NHC CH$_2$), 4.99 (hept, J = 6.7 Hz, 2H, −CHR$_2$), 4.56−4.36 (m, 2H, cod CH), 3.77−3.55 (m, 2H, cod CH), 2.42−2.23 (m, 4H, cod CH$_2$), 2.22−2.06 (m, 2H, cod CH$_2$), 1.99 (m, 2H, cod CH$_2$), 1.47 (d, J = 6.7 Hz, 6H, −CH$_3$), 0.60 (d, J = 6.7 Hz, 3H, −CH$_3$). ^{13}C{^{1}H} NMR (126 MHz, CD$_2$Cl$_2$): δ 170.81 (d, J = 10.0), 134.37 (d, J = 10.9), 131.88, 130.87 (d, J = 50.2), 129.58 (d, J = 10.0), 119.65, 85.99 (d, J = 12.0), 80.25, 31.60 (d, J = 1.8), 30.91 (d, J = 3.0), 25.06, 21.77. ^{31}P{^{1}H} NMR (202 MHz, CD$_2$Cl$_2$): δ 18.22, −144.52 (hept, J = 710.4 Hz). Anal. Calcd for C$_{35}$H$_{43}$F$_6$IrN$_2$P$_2$: C, 48.89; H, 5.04; N, 3.26. Found: C, 49.02; H, 4.77; N, 3.16.

mer,trans-Bis[triphenylphosphine](_N,N_-dimethylbenzimidazol-2-ylidene)trihydridoiridium (2). In a flame-dried Schlenk flask was added [$η^4$-1,5-cyclooctadiene][triphenylphosphine](_N,N_-dimethyl-benzimidazol-2-ylidene)iridium hexafluorophosphate (1a; 442.8 mg, 0.5185 mmol) and PPh$_3$ (135.9 mg, 0.5185 mg).The flask was evacuated and back-filled with nitrogen three times. Freshly distilled and degassed 1,8-diazabicyclo[5.4.0]undec-7-ene (DBU; 77.3 mL, 0.5185 mmol) was added via syringe to the solid. Dried degassed toluene (3 mL) was added

to the flask. After three freeze−pump−thaw cycles, the solution was cooled to −78 °C. Hydrogen was introduced, and the reaction mixture was warmed to room temperature. The reaction mixture was stirred for 22 h, during which time the suspension became a pale yellow solution. Hydrogen flow was stopped, and the reaction flask was rapidly evacuated and back-filled with nitrogen gas. The solution was filtered through Celite in vacuo, and the solvent was evaporated under vacuum. The material was recrystallized from dichloromethane and diethyl ether to afford a bright yellow solid (167.7 mg, 37% yield after recrystallization). ^{1}H NMR (500 MHz, CD$_2$Cl$_2$): δ 7.75−7.61 (m, 12H, PPh$_3$ CH), 7.16−7.07 (m, 18H, PPh$_3$ CH), 7.00−6.92 (m, 2H, NHC −CH−), 6.85−6.78 (m, 2H, NHC −CH−), 3.37 (s, 6H, N−CH$_3$), −11.08 (td, J_{PH} = 17.6 Hz, J_{HH} = 4.4 Hz, 2H, Ir−H), −13.86 (tt, J_{PH} = 19.3 Hz, J_{HH} = 4.4 Hz, 1H, Ir−H). ^{13}C{^{1}H} NMR (126 MHz, CD$_2$Cl$_2$): δ 189.45 (m), 139.52 (t, J = 25.6 Hz), 134.87, 134.49 (t, J = 6.5 Hz), 129.14, 127.66 (t, J = 4.8 Hz), 121.54, 109.70, 37.38. ^{31}P{^{1}H} NMR (202 MHz, CD$_2$Cl$_2$): δ 26.11. IR (CH$_2$Cl$_2$, cm^{-1}): 2001.9 ($ν_{Ir−H}$), 1760.6 ($ν_{Ir−H}$). Anal. Calcd for C$_{45}$H$_{43}$IrN$_2$P$_2$·H$_2$O: C, 61.14; H, 5.13; N, 3.17. Found: C, 60.89; H, 4.75; N, 3.21.

Bis[triphenylphosphine](_N,N_-dimethylbenzimidazol-2-ylidene)-dihydridoiridium Hexafluorophosphate (4). In a flame-dried Schlenk flask was added [$η^4$-1,5-cyclooctadiene][triphenylphosphine](_N,N_-dimethylbenzimidazol-2-ylidene)iridium hexafluorophosphate (1a; 100.0 mg, 0.117 mmol) and PPh$_3$ (30.5 mg, 0.117 mmol). The flask was evacuated and back-filled with nitrogen three times. Dried degassed tetrahydrofuran (3 mL) was added to the flask. The solution was cooled to 0 °C and stirred for 5 min. Hydrogen gas was actively bubbled through the solution. The reaction mixture was stirred for 2 h, during which time a white solid precipitated from the solution. Hydrogen flow was stopped, and the reaction mixture was rapidly evacuated and back-filled with nitrogen gas. The solution was decanted, and the remaining solid was rinsed with THF under a nitrogen atmosphere at −78 °C. The washed solid was subjected to vacuum, at which point the solid changed color from white to orange. The crude material was recrystallized from dichloromethane and diethyl ether at 0 °C to afford the orange product (50.2 mg, 42% yield after recrystallization). Crystals suitable for X-ray diffraction studies were grown from a solution of dichloromethane layered with diethyl ether at 0 °C under a nitrogen atmosphere. ^{1}H NMR (500 MHz, DCE-d_4): δ 7.49−7.20 (m, 32H, PPh$_3$ CH, NHC−CH−), 7.06−7.00 (m, 2H, NHC −CH−), 3.02 (s, 6H, N−CH$_3$), −20.67 (s, 2H, Ir−H). ^{13}C{^{1}H} NMR (126 MHz, DCE-d_4): δ 134.87, 134.11, 133.54, 132.96 (t, J = 26.6 Hz), 131.84, 131.15, 129.17, 129.03, 123.40, 109.99, 34.38. Attempts to locate the C2 NHC resonance by modifying the spectrometer decoupling strength and frequency were unsuccessful. ^{31}P{^{1}H} NMR (202 MHz, DCE-d_4): δ 27.38, −144.55 (hept, J = 710.3 Hz). IR (thin film, cm^{-1}): 1981.5 cm^{-1} ($ν_{Ir−H}$). Anal. Calcd for C$_{45}$H$_{42}$F$_6$IrN$_2$P$_3$: C, 53.52; H, 4.19; N, 2.77. Found: C, 53.29; H, 3.98; N, 2.86.

Spectroscopic Observation of 3a. Complex **4** (5.0 mg, 0.0050 mmol) was placed in a J. Young NMR tube in a glovebox. The tube was subjected to vacuum and back-filled with hydrogen gas. The orange solid immediately became white. Degassed DCM-d_2 (0.7 mL) was added to the NMR tube under an inert atmosphere, and the sample was immediately used in spectroscopic studies. ^{1}H NMR (500 MHz, CD$_2$Cl$_2$): δ 7.57−7.28 (m, 18H), 7.28−7.21 (m, 14H), 7.13−6.93 (m, 2H), 3.11 (s, 6H), −7.77 (s, 4H). ^{13}C{^{1}H} NMR (126 MHz, CD$_2$Cl$_2$): δ 177.35 (m), 134.36, 133.86, 133.58 (t, J = 6.3 Hz), 133.40, 131.56, 129.11 (t, J = 5.3 Hz), 124.15, 111.06, 36.98. ^{31}P{^{1}H} NMR (202 MHz, CD$_2$Cl$_2$): δ 10.33, −144.55 (hept, J = 710.2 Hz).

Spectroscopic Observation of 3b. Complex **2** (5.0 mg, 0.0058 mmol) was placed in a J. Young NMR tube in a glovebox, followed by degassed DCM-d_2 (0.7 mL). [H(Et$_2$O)$_2$][BAr$^F_4$] (5.8 mg, 0.0057 mmol) was then added as a solid to the tube. The sample was immediately used in inversion recovery experiments. The NMR spectra

7559

dx.doi.org/10.1021/ja2014983 |_J. Am. Chem. Soc._ 2011, 133, 7547–7562

of the cation are identical with those reported for **3a**. The BAr$^F_4$ form of salt **4** was generated by gently applying a vacuum to this sample; its identity was confirmed by ^{1}H and ^{31}P NMR.

Optimized Procedure for Catalytic Quinoline Hydrogenation.
(a) 1 atm Pressure. In a flame-dried Schlenk flask under air was added a stir bar, catalyst **1a** (4.4 mg, 0.0052 mmol), PPh$_3$ (1.36 mg, 0.0052 mmol), and substrate (0.52 mmol). Dried degassed toluene (2 mL) was added. The flask was rapidly evacuated by vacuum and back-filled with hydrogen gas three times, and the flask was kept under ambient hydrogen pressure during the reaction. The reaction mixture was then heated to 35 °C and stirred for 18 h, after which time the solution was passed through basic alumina to afford the crude product. Conversion was assessed by ^{1}H NMR integration of product and any starting material remaining and normalizing to 100%. The tetrahydroquinoline products can be isolated by silica gel chromatography (hexanes/ethyl acetate). The spectra of the known compounds isolated using this method (2-methyl-1,2,3,4-tetrahydroquinoline,[12] 2-ethyl-1,2,3,4-tetrahydroquinoline,[12] 2-butyl-1,2,3,4-tetrahydroquinoline,[12] 2-phenyl-1,2,3,4-tetrahydroquinoline,[12] 2,6-dimethyltetrahydroquinoline,[12] 1,2,3,4-tetrahydrobenzo[*h*]quinoline,[4,44] and *N*-benzylaniline[45]) matched literature values.

(b) 5 atm Pressure. In a glass reactor sleeve under air was added a stir bar, catalyst **1a** (4.4 mg, 0.0052 mmol), PPh$_3$ (1.36 mg, 0.0052 mmol), and substrate (0.52 mmol). Dried degassed toluene (2 mL) was added. The sleeve was inserted into the reactor vessel, and the reactor was assembled under air. The reactor was purged by pressurizing the apparatus to 5 atm and venting three times. The reactor was pressurized to 5 atm and heated to 35 °C and the mixture stirred for 18 h, after which the reactor was vented. The reaction solution was passed through basic alumina to afford the crude product. Conversion was assessed by ^{1}H NMR integration of product and any starting material remaining and normalizing to 100%. The tetrahydroquinoline products can be isolated by silica gel chromatography (hexanes/ethyl acetate). The spectra of the known compounds isolated using this method (8-chloro-2-methyl-1,2,3,4-tetrahydroquinoline,[9] 6-bromo-1,2,3,4-tetrahydroquinoline,[46] and 1,2,3,4-tetrahydroquinoline[47]) matched literature values.

Catalytic Experiment with Complex 2 without [H(Et$_2$O)$_2$]-[BAr$^F_4$]. Complex **2** (3.0 mg, 0.0035 mmol, 0.01 equiv) was placed into a flame-dried Schlenk flask under a nitrogen atmosphere. A degassed solution of 2-methylquinoline (47 μL, 0.35 mmol) in toluene (3 mL) was added to the flask via syringe. The flask was placed under vacuum and rapidly back-filled with hydrogen gas three times. The reaction mixture was stirred for 16 h at 35 °C. The ^{1}H NMR spectrum of an aliquot of the reaction mixture confirmed that no conversion to product occurred.

Catalytic Experiment with Complex 2 and [H(Et$_2$O)$_2$]-[BAr$^F_4$]. Complex **2** (3.7 mg, 0.0043 mmol, 0.01 equiv) and [H(Et$_2$O)$_2$][BAr$^F_4$] (4.0 mg, 0.0043 mmol, 0.01 equiv) were placed in a flame-dried Schlenk flask under a nitrogen atmosphere. A degassed solution of 2-methylquinoline (39 μL, 0.43 mmol) in toluene (3 mL) was added to the flask via syringe. The flask was placed under vacuum and rapidly back-filled with hydrogen gas three times. The reaction mixture was stirred for 16 h at 35 °C. Formation of the 2-methyltetrahydroquinoline product was confirmed by ^{1}H NMR of a reaction aliquot.

Catalytic Experiment with Complex 4. Complex **4** (3.5 mg, 0.0035 mmol, 0.01 equiv) was added to a flame-dried Schlenk flask under a nitrogen atmosphere. A degassed solution of 2-methylquinoline (47 μL, 0.347 mmol) in toluene (2 mL) was added to the flask via syringe. The flask was placed under vacuum and rapidly back-filled with hydrogen gas three times. The reaction mixture was stirred for 16 h at 35 °C. Formation of the 2-methyltetrahydroquinoline product was confirmed by ^{1}H NMR of a reaction aliquot.

Stoichiometric Experiment with Complex 2, [H(Et$_2$O)$_2$][BAr$^F_4$], and 2-Methylquinoline. Complex **2** (8.0 mg, 0.0092 mmol) and [H(Et$_2$O)$_2$][BAr$^F_4$] (9.5 mg, 0.0094 mmol) were placed in a flame-dried Schlenk tube under a nitrogen atmosphere. A degassed solution of 2-methylquinoline (1.5 μL, 0.0092 mmol) in toluene (0.75 mL) was added to the tube via syringe. The proton NMR spectrum of the tube indicated that no 2-methylquinoline had been formed. The tube was then placed under vacuum and rapidly back-filled with hydrogen gas three times. The reaction mixture was allowed to stand for 16 h at room temperature. Formation of the 2-methyltetrahydroquinoline product was confirmed by ^{1}H NMR.

Stoichiometric Experiment with Complex 2, [H(Et$_2$O)$_2$][BAr$^F_4$], and Acridine. Complex **2** (8.7 mg, 0.0010 mmol) and [H(Et$_2$O)$_2$][BAr$^F_4$] (10.1 mg, 0.0010 mmol) were placed in a flame-dried J. Young tube under a nitrogen atmosphere. DCM-d_2 (0.75 mL) was placed in the tube, and acridine (2.0 mg, 0.011 mmol) was added as a solid. The ^{1}H NMR spectrum of the sample indicated that 9,10-dihydroacridine had been formed.

Decomposition of Complex 4 in Dichloromethane. A solution of **4** in dichloromethane was stored under nitrogen for 1 week at room temperature. The solvent was reduced under vacuum, and the residual yellow solid was recrystallized (dichloromethane/diethyl ether) to afford a mixture of **4** and X-ray-quality crystals of chlorobis-[triphenylphosphine](*N*,*N*-dimethylbenzimidazol-2-ylidene)hydridoiridium hexafluorophosphate. Spectra of the decomposition product: ^{1}H NMR (500 MHz, CD$_2$Cl$_2$) δ 7.51−7.14 (m, 33H), 6.84 (d, *J* = 8.1 Hz, 1H), 3.46 (s, 3H), 2.07 (s, 3H), −40.29 (t, *J* = 13.3 Hz, 1H); ^{31}P{^{1}H} NMR (202 MHz, CD$_2$Cl$_2$) δ 23.94 (s), −144.55 (sept).

Inversion Recovery (T_1) Experiments. Samples were prepared in J. Young NMR tubes under an inert atmosphere. All spectra were collected using a Bruker 500 MHz NMR spectrometer equipped for variable-temperature studies. Relative integrations were collected, and individual T_1 values determined, for each observed hydride signal. For each sample, an inversion recovery pulse sequence was performed at various evolution periods, *t*, between an initial 180° pulse and a second 90° pulse. This experiment was performed at several different temperatures in order to estimate T_1(min). Integration of hydride signals was performed after a Fourier transform, phase correction, and baseline correction of the unprocessed NMR spectra. T_1 values were obtained from this data by plotting relative integration versus evolution period and fitting the data according to

$$I(t) = I(0) + Ae^{-t/T_1}$$

where $I(t)$ is integration at evolution period *t*, T_1 is the spin−lattice relaxation time, and *A* is a constant.

Computational Details. Two different models of the Ir complex were used in this study: one using the full system with the DFT/MM methodology ONIOM, and the other replacing the real carbene C$_6$H$_4$-(NMe)$_2$C and PPh$_3$ by C$_2$H$_2$(NMe)$_2$C and PH$_3$, respectively. The first level was used for the structural determination of **2** and the cations of **3a** and **4** and the second level for the mechanistic study of the hydrogenation of 2-methylquinoline. In the ONIOM calculations the Ph groups of the phosphines were included in the MM part. All optimizations were performed with the Gaussian09 program[48] with the functional B3PW91[49] for the DFT level and the force field UFF for the molecular mechanics level. For the DFT partition, the basis set used was the ECP-adapted SDDALL[50] with a set of polarization functions for Ir[51] and P[52] and the all-electron 6-31G(d,p)[53] for N, C, and H. All structures were fully optimized without any geometry or symmetry constraint.

In the mechanistic study using the model system, at full DFT level, each stationary point was classified as a minimum or transition state by analytical calculation of the frequencies. The connection between reactant and product through a given transition state was checked by optimization of slightly altered geometries of the transition state along the two directions of the transition state vector associated with the imaginary frequency. Entropy effects calculated in the gas phase at 298 K and 1 atm from harmonic approximation of frequencies were included in order to compare the inner- and outer-sphere mechanisms, since the

former is unimolecular, whereas the latter is bimolecular. In addition, the effect of toluene solvent (ε = 2.379) was included by using the continuum SMD model[54] with single-point 6-311+G** calculations and the methodology proposed by Maseras et al.[55] for the Gibbs energy in solution.

In the calculations considering the full system, which have been used to evaluate the relative stability of the different isomers of the cation of **3a**, the entropy was not considered, since all isomers have the same molecularity. In this case, the energies given in the text are potential energies in solution obtained by single-point 6-311+G** calculations from the ONIOM geometries using the M06 functional.[56] This methodology has been used to consider the dispersion of the aromatic rings present in the carbene and the phosphine.

■ ASSOCIATED CONTENT

ⓢ Supporting Information.   Text, tables, figures, and CIF files giving details of the X-ray analysis of **1a**, **4**, iodo[η^4-1,5-cyclooctadiene](*N,N*-dimethylbenzimidazol-2-ylidene)iridium, and chlorobis[triphenylphosphine](*N,N*-dimethylbenzimidazol-2-ylidene)hydridoiridium hexafluorophosphate, complete inversion recovery data, the full list of authors for ref 48, and Cartesian coordinates of all optimized structures with the corresponding energies. This material is available free of charge via the Internet at http://pubs.acs.org.

■ AUTHOR INFORMATION

Corresponding Author
robert.crabtree@yale.edu; odile.eisenstein@univ-montp2.fr

Present Addresses
§Institute of Chemical Research of Catalonia (ICIQ), av. Països Catalans, 16, 43007 Tarragona, Catalonia, Spain.

■ ACKNOWLEDGMENT

■ REFERENCES

(1) Katritzky, A. R.; Rachwal, S.; Rachwal, B. *Tetrahedron* **1996**, *52*, 15031–15070.

(2) (a) Moores, A.; Poyatos, M.; Luo, Y.; Crabtree, R. H. *New J. Chem.* **2006**, *30*, 1675–1678. (b) Clot, E.; Eisenstein, O.; Crabtree, R. H. *Chem. Commun.* **2007**, 2231–2233. (c) Crabtree, R. H. *Energy Environ. Sci.* **2008**, *1*, 134–138. (d) Dean, D.; Davis, B.; Jessop, P. G. *New J. Chem.* **2011**, *35*, 417–422.

(3) (a) Jardine, I.; McQuillin, F. J. *J. Chem. Soc. D* **1970**, 626a–626a. (b) Laine, R. M. *New J. Chem.* **1987**, *11*, 543–547. (c) Sánchez-Delgado, R. A.; González, E. *Polyhedron* **1989**, *8*, 1431–1436. (d) Baralt, E.; Smith, S. J.; Hurwitz, J.; Horvath, I. T.; Fish, R. H. *J. Am. Chem. Soc.* **1992**, *114*, 5187–5196. (e) Rosales, M.; Alvarado, Y.; Boves, M.; Rubio, R.; Soscún, H.; Sánchez-Delgado, R. A. *Transition Met. Chem. (London)* **1995**, *20*, 246–251. (f) Glorius, F.; Spielkamp, N.; Holle, S.; Goddard, R.; Lehmann, C. W. *Angew. Chem., Int. Ed.* **2004**, *43*, 2850–2852. (g) Legault, C. Y.; Charette, A. B. *J. Am. Chem. Soc.* **2005**, *127*, 8966–8967. (h) Rosales, M.; Vallejo, R.; Soto, J.; Chacón, G.; González, Á.;

González, B. *Catal. Lett.* **2006**, *106*, 101–105. (i) Lu, S. M.; Han, X. W.; Zhou, Y. G. *J. Organomet. Chem.* **2007**, *692*, 3065–3069.

(4) Fish, R. H.; Thormodsen, A. D.; Cremer, G. A. *J. Am. Chem. Soc.* **1982**, *104*, 5234–5237.

(5) Sanchez-Delgado, R. A.; Rondon, D.; Andriollo, A.; Herrera, V.; Martin, G.; Chaudret, B. *Organometallics* **1993**, *12*, 4291–4296.

(6) Yamaguchi, R.; Ikeda, C.; Takahashi, Y.; Fujita, K.-I. *J. Am. Chem. Soc.* **2009**, *131*, 8410–8412.

(7) (a) Eggenstein, M.; Thomas, A.; Theuerkauf, J.; Franciò, G.; Leitner, W. *Adv. Synth. Catal.* **2009**, *351*, 725–731. (b) Li, Z. W.; Wang, T. L.; He, Y. M.; Wang, Z. J.; Fan, Q. H.; Pan, J.; Xu, L. J. *Org. Lett.* **2008**, *10*, 5265–5268.

(8) Zhou, H.; Li, Z.; Wang, Z.; Wang, T.; Xu, L.; He, Y.; Fan, Q.-H.; Pan, J.; Gu, L.; Chan, A. S. C. *Angew. Chem., Int. Ed.* **2008**, *47*, 8464–8467.

(9) Gou, F. R.; Wei, L.; Zhang, Z.; Liang, Y. M. *Adv. Synth. Catal.* **2010**, *352*, 2441–2444.

(10) (a) Lu, S. M.; Bolm, C. *Adv. Synth. Catal.* **2008**, *350* 1101–1107. (b) Zhou, Y.-G. *Acc. Chem. Res.* **2007**, *40*, 1357–1366. (c) Yamagata, T.; Tadaoka, H.; Nagata, M.; Hirao, T.; Kataoka, Y.; Ratovelomanana-Vidal, V.; Genet, J.-P.; Mashima, K. *Organometallics* **2006**, *25*, 2505–2513. (d) Tadaoka, H.; Cartigny, D.; Nagano, T.; Gosavi, T.; Ayad, T.; Genet, J.-P.; Ohshima, T.; Ratovelomanana-Vidal, V.; Mashima, K. *Chem. Eur. J.* **2009**, *15*, 9990–9994. (e) Reetz, M. T.; Li, X. *Chem. Commun.* **2006**, 2159–2160.

(11) (a) Mrsic, N.; Lefort, L.; Boogers, J. A. F.; Minnaard, A. J.; Feringa, B. L.; de Vries, J. G. *Adv. Synth. Catal.* **2008**, *350*, 1081–1089. (b) Deport, C.; Buchotte, M.; Abecassis, K.; Tadaoka, H.; Ayad, T.; Ohshima, T.; Genet, J.-P.; Mashima, K.; Ratovelomanana-Vidal, V. *Synlett* **2007**, 2743–2747. (c) Núñez-Rico, J. L.; Fernández-Pérez, H.; Benet-Buchholz, J.; Vidal-Ferran, A. *Organometallics* **2010**, *29*, 6627–6631.

(12) Wang, W.-B.; Lu, S.-M.; Yang, P.-Y.; Han, X.-W.; Zhou, Y.-G. *J. Am. Chem. Soc.* **2003**, *125*, 10536–10537.

(13) Wang, D.-W.; Wang, X.-B.; Wang, D.-S.; Lu, S.-M.; Zhou, Y.-G.; Li, Y.-X. *J. Org. Chem.* **2009**, *74*, 2780–2787.

(14) Qiu, L.; Kwong, F. Y.; Wu, J.; Lam, W. H.; Chan, S.; Yu, W. Y.; Li, Y. M.; Guo, R.; Zhou, Z.; Chan, A. S. C. *J. Am. Chem. Soc.* **2006**, *128*, 5955–5965.

(15) Bianchini, C.; Meli, A.; Vizza, F. *Eur. J. Inorg. Chem.* **2001**, *2001*, 43–68.

(16) (a) Balcells, D.; Nova, A.; Clot, E.; Gnanamgari, D.; Crabtree, R. H.; Eisenstein, O. *Organometallics* **2008**, *27*, 2529–2535. (b) Noyori, R.; Hashiguchi, S. *Acc. Chem. Res.* **1997**, *30*, 97–102. Comas-Vives, A.; Ujaque, G.; Lledós, A. *Organometallics* **2008**, *27*, 4854–4863. (c) Comas-Vives, A.; Ujaque, G.; Lledós, A. *J. Mol. Struct. (THEOCHEM)* **2009**, *903*, 123–132. (d) Chen, Y.; Tang, Y.; Lei, M. *Dalton Trans.* **2009**, 2359–2364. (e) Wu, J.; Liu, J.; Di Tommaso, D.; Iggo, J. A.; Catlow, C. R. A.; Bacsa, J.; Xiao, J. *Chem. Eur. J.* **2008**, *14*, 7699–7715. (f) Leyssens, T.; Peeters, D.; Harvey, J. N. *Organometallics* **2008**, *27*, 1514–1523. (g) Yamakawa, M.; Ito, H.; Noyori, R. *J. Am. Chem. Soc.* **2000**, *122*, 1466–1478. (h) Samec, J. S. M.; Bäckvall, J.-E.; Andersson, P. G.; Brandt, P. *Chem. Soc. Rev.* **2006**, *35*, 237–248. (i) Clapham, S. E.; Hadzovic, A.; Morris, R. H. *Coord. Chem. Rev.* **2004**, *248*, 2201–2237. (k) Casey, C. P.; Johnson, J. B.; Singer, S. W.; Cui, Q. *J. Am. Chem. Soc.* **2005**, *127*, 3100–3109. (l) Privalov, T.; Samec, J. S. M.; Bäckvall, J.-E. *Organometallics* **2007**, *26*, 2840–2848. (m) Nova, A.; Balcells, D.; Schley, N. D.; Dobereiner, G. E.; Crabtree, R. H.; Eisenstein, O. *Organometallics* **2010**, *29*, 6548–6558.

(17) Rosales, M.; Vallejo, R.; Soto, J.; Bastidas, L.; Molina, K.; Baricelli, P. *Catal. Lett.* **2010**, *134*, 56–62.

(18) Bianchini, C.; Barbaro, P.; Macchi, M.; Meli, A.; Vizza, F. *Helv. Chim. Acta* **2001**, *84*, 2895–2923.

(19) Rosales, M.; Boves, M.; Soscún, H.; Ruette, F. *J. Mol. Struct. (THEOCHEM)* **1998**, *433*, 319–328.

(20) Crabtree, R. H. *The Organometallic Chemistry of the Transition Metals*, 5th ed.; Wiley: New York, 2009.

(21) While this paper was in press, an (NHC)Ru-catalyzed hydrogenation of quinoxaline carbocyclic rings was reported. Urban, S.; Ortega, N.; Glorius, F. *Angew. Chem. Int. Ed.* **2011**, *50*, 3803−3806.

(22) (a) Jeletic, M. S.; Jan, M. T.; Ghiviriga, I.; Abboud, K. A.; Veige, A. S. *Dalton Trans.* **2009**, 2764–2776. (b) Vazquez-Serrano, L. D.; Owens, B. T.; Buriak, J. M. *Inorg. Chim. Acta* **2006**, *359*, 2786–2797. (c) Page, M. J.; Wagler, J.; Messerle, B. A. *Dalton Trans.* **2009** 7029–7038.

(23) Vazquez-Serrano, L. D.; Owens, B. T.; Buriak, J. M. *Chem. Commun.* **2002**, 2518–2519.

(24) Crabtree, R. H. *Acc. Chem. Res.* **1979**, *12*, 331–337.

(25) Köcher, C.; Herrmann, W. A. *J. Organomet. Chem.* **1997**, *532*, 261–265.

(26) Lin, I. J. B.; Vasam, C. S. *Coord. Chem. Rev.* **2007**, *251*, 642–670.

(27) Brown, J. A.; Irvine, S.; Kennedy, A. R.; Kerr, W. J.; Andersson, S.; Nilsson, G. N. *Chem. Commun.* **2008**, 1115–1117.

(28) Lightfoot, A.; Schnider, P.; Pfaltz, A. *Angew. Chem., Int. Ed.* **1998**, *37*, 2897–2899. Roseblade, S. J.; Pfaltz, A. *C. R. Chim.* **2007**, *10*, 178–187.

(29) Tanaka, R.; Yamashita, M.; Nozaki, K. *J. Am. Chem. Soc.* **2009**, *131*, 14168–14169.

(30) (a) Clarke, Z. E.; Maragh, P. T.; Dasgupta, T. P.; Gusev, D. G.; Lough, A. J.; Abdur-Rashid, K. *Organometallics* **2006**, *25*, 4113–4117. (b) Choualeb, A.; Lough, A. J.; Gusev, D. G. *Organometallics* **2007**, *26*, 5224–5229.

(31) Brookhart, M.; Grant, B.; Volpe, A. F. *Organometallics* **1992**, *11*, 3920–3922.

(32) (a) Maseras, F.; Lledós, A.; Clot, E.; Eisenstein, O. *Chem. Rev.* **2000**, *100*, 601–636. (b) Hebden, T. J.; Goldberg, K. I.; Heinekey, D. M.; Zhang, X.; Emge, T. J.; Goldman, A. S.; Krogh-Jespersen, K. *Inorg. Chem.* **2010**, *49*, 1733–1742.

(33) Crabtree, R. H. *Acc. Chem. Res.* **1990**, *23*, 95–101.

(34) Yao, W.; Faller, J. W.; Crabtree, R. H. *Inorg. Chim. Acta* **1997**, *259*, 71–76.

(35) (a) Gründemann, S.; Kovacevic, A.; Albrecht, M.; Faller, J. W.; Crabtree, R. H. *J. Am. Chem. Soc.* **2002**, *124*, 10473–10481. (b) Gründemann, S.; Kovacevic, A.; Albrecht, M.; Faller, J. W.; Crabtree, R. H. *Chem. Commun.* **2001**, 2274–2275. (c) Chianese, A. R.; Kovacevic, A.; Zeglis, B. M.; Faller, J. W.; Crabtree, R. H. *Organometallics* **2004**, *23*, 2461–2468.

(36) Peris, E.; Lee, J. C.; Rambo, J. R.; Eisenstein, O.; Crabtree, R. H. *J. Am. Chem. Soc.* **1995**, *117*, 3485–3491.

(37) Herde, J. L.; Lambert, J. C.; Senoff, C. V. *Inorg. Synth.* **1974**, *15*, 18–19.

(38) Yakelis, N. A.; Bergman, R. G. *Organometallics* **2005**, *24*, 3579–3581.

(39) Lachance, N.; Roy, P.; Leblanc, Y. U.S. Patent 20050277644, 2005.

(40) Zinner, S. C.; Rentzsch, C. F.; Herdtweck, E.; Herrmann, W. A.; Kuhn, F. E. *Dalton Trans.* **2009**, 7055–7062.

(41) Amyes, T. L.; Diver, S. T.; Richard, J. P.; Rivas, F. M.; Toth, K. *J. Am. Chem. Soc.* **2004**, *126*, 4366–4374.

(42) Huang, W.; Guo, J.; Xiao, Y.; Zhu, M.; Zou, G.; Tang, J. *Tetrahedron* **2005**, *61*, 9783–9790.

(43) Frey, G. D.; Rentzsch, C. F.; von Preysing, D.; Scherg, T.; Mühlhofer, M.; Herdtweck, E.; Herrmann, W. A. *J. Organomet. Chem.* **2006**, *691*, 5725–5738.

(44) Scheurer, H.; Zsindely, J.; Schmid, H. *Helv. Chim. Acta* **1973**, *56*, 478–489.

(45) Hollmann, D.; Bähn, S.; Tillack, A.; Beller, M. *Angew. Chem., Int. Ed.* **2007**, *46*, 8291–8294.

(46) Sahin, A.; Cakmak, O.; Demirtas, I.; Okten, S.; Tutar, A. *Tetrahedron* **2008**, *64*, 10068–10074.

(47) Ortiz-Marciales, M.; Rivera, L. D.; De Jesús, M.; Espinosa, S.; Benjamin, J. A.; Casanova, O. E.; Figueroa, I. G.; Rodríguez, S.; Correa, W. *J. Org. Chem.* **2005**, *70*, 10132–10134.

(48) Frisch, M. J. et al. *GAUSSIAN 09 Rev. A.02*; Gaussian, Inc., Wallingford, CT, 2009.

(49) (a) Becke, A. D. *J. Chem. Phys.* **1993**, *98*, 5648–5662. (b) Perdew, J. P.; Wang, Y. *Phys. Rev. B* **1992**, *45*, 13244–13249.

(50) (a) Andrae, D.; Häussermann, U.; Dolg, M.; Stoll, H.; Preuss, H. *Theor. Chim. Acta* **1990**, *77*, 123–141. (b) Bergner, A.; Dolg, M.; Küchle, W.; Stoll, H.; Preuss, H. *Mol. Phys.* **1993**, *80*, 1431–1441.

(51) Ehlers, A. W.; Böhme, M.; Dapprich, S.; Gobbi, A.; Höllwarth, A.; Jonas, V.; Köhler, K. F.; Stegmann, R.; Veldkamp, A.; Frenking, G. *Chem. Phys. Lett.* **1993**, *208*, 111–114.

(52) Höllwarth, A.; Böhme, H.; Dapprich, S.; Ehlers, A. W.; Gobbi, A.; Jonas, V.; Köhler, K. F.; Stegmann, R.; Veldkamp, A.; Frenking, G. *Chem. Phys. Lett.* **1993**, *203*, 237–240.

(53) Hariharan, P. C.; Pople, J. A. *Theor. Chim. Acta* **1973**, *28*, 213–222.

(54) Marenich, A. V.; Cramer, C. J.; Truhlar, D. G. *J. Phys. Chem. B* **2009**, *113*, 6378–6396.

(55) (a) Balcells, D.; Ujaque, G.; Fernandez, I.; Khiar, N.; Maseras, F. *J. Org. Chem.* **2006**, *71*, 6388–6396. (b) Braga, A. A. C.; Ujaque, G.; Maseras, F. *Organometallics* **2006**, *25*, 3647–3658.

(56) Zhou, Y.; Truhlar, D. G. *Theor. Chem. Acc.* **2008**, *120*, 215–241.

7562

dx.doi.org/10.1021/ja2014983 |*J. Am. Chem. Soc.* 2011, 133, 7547–7562